Changes in local mineral homeostasis facilitate the formation of benign and malignant testicular microcalcifications

Ida Marie Boisen[1,2], Nadia Krarup Knudsen[1], John Erik Nielsen[3], Ireen Kooij[1], Mathilde Louise Bagger[1], Jovana Kaludjerovic[4], Peter J. O'Shaughnessy[5], Peter W. Andrews[6], Noriko Ide[4], Birgitte Grønkær Toft[7], Anders Juul[3], Arnela Mehmedbašić[1], Anne Jørgensen[1], Lee B. Smith[8], Richard W. Norman[9], Ewa Rajpert-De Meyts[3], Beate Lanske[4], Martin Blomberg Jensen[1]*

1: Division of Translational Endocrinology, Department of Endocrinology and Internal Medicine, University Hospital Copenhagen, Herlev-Gentofte, DK-2730 Herlev, Denmark

2: Group of Skeletal, Mineral, and Gonadal Endocrinology, Department of Growth and Reproduction, Rigshospitalet, University of Copenhagen, DK-2100 Copenhagen, Denmark

3: Department of Growth and Reproduction, Rigshospitalet, University of Copenhagen, DK-2100 Copenhagen, Denmark

4: Division of Bone and Mineral Research, Harvard School of Dental Medicine/Harvard Medical School, Harvard University, Boston, MA 02108, US

5: College of Medical, Veterinary and Life Sciences, Institute of Biodiversity, Animal Health and Comparative Medicine, University of Glasgow, G61 1QH, Glasgow, UK

6: Centre for Stem Cell Biology, Department of Biomedical Science, University of Sheffield, Western Bank, Sheffield S10 2TN, UK

7: Department of Pathology, Rigshospitalet, DK-2100 Copenhagen, Denmark

8: MRC Centre for Reproductive Health, University of Edinburgh, The Queen's Medical Research Institute, 47 Little France Crescent, Edinburgh, EH16 4TJ, UK

9: Department of Urology, Dalhousie University, Halifax NS B3H 2Y9, Nova Scotia, Canada

Keywords: FGF23, microcalcifications, testicular germ cell cancer, reproduction, testis

Abstract: 249 words

Word count: 4814

Figures: 8

Tables: 0

*Address for correspondence

Martin Blomberg Jensen

Martin.blomberg.jensen@regionh.dk

All authors declare no conflicts of interests

Abstract

Testicular microcalcifications consist of hydroxyapatite and have been associated with an increased risk of testicular germ cell tumors (TGCTs) but may also be the result of benign causes such as loss-of-function variants in the phosphate-transporter gene *SLC34A2*. Here, we show that fibroblast growth factor 23 (FGF23), a regulator of phosphate homeostasis, is expressed in testicular germ cell neoplasia *in situ* (GCNIS), embryonal carcinoma (EC), and human embryonic stem cells. FGF23 is not glycosylated in TGCTs and therefore cleaved into a C-terminal fragment which competitively antagonizes full-length FGF23. Here, *Fgf23* knockout mice presented with marked calcifications in the epididymis, spermatogenic arrest, and focally germ cells expressing the osteoblast marker bone gamma-carboxyglutamate protein (BGLAP). Moreover, the frequent testicular microcalcifications in mice with no functional androgen receptor and lack of circulating gonadotropins is associated with lower *Slc34a2* and higher *Slc34a1/Bglap* expression compared with wild-type mice. In accordance, human testicular specimens with microcalcifications also have lower *SLC34A2* and a subpopulation of germ cells express SLC34A1, BGLAP, and RUNX2 highlighting aberrant local phosphate handling and expression of bone-specific proteins. Mineral disturbance *in vitro* using calcium or phosphate treatment induced deposition of calcium-phosphate in a spermatogonial cell line and this effect was fully rescued by the mineralization-inhibitor pyrophosphate. In conclusion, testicular microcalcifications may arise secondary to local alterations in mineral homeostasis, which in combination with impaired Sertoli cell function and reduced levels of mineralization-inhibitors due to high alkaline phosphatase activity in GCNIS and TGCTs, facilitate osteogenic-like differentiation of testicular cells and deposition of hydroxyapatite.

Introduction

Testicular microlithiasis in infertile men is associated with an increased risk of testicular germ cell tumors (TGCTs)[1–4]. However, both ultrasonic and histological microcalcifications are also frequent findings in the testis of asymptomatic men and the etiology remains largely unknown in both malignant and benign cases. The histological microcalcifications have been shown by Raman spectroscopy to consist of hydroxyapatite[5,6], which is normally found exclusively in the skeleton and requires the presence of cells with osteoblast-like characteristics[7,8]. Extra-skeletal mineralization is often caused by an imbalance in promoters and inhibitors of biomineralization[7,9–11]. Tissue mineralization is tightly controlled by small integrin-binding ligand N-linked glycoproteins (SIBLINGs) such as osteopontin (OPN) and dentin matrix acidic phosphoprotein 1 (DMP1) that regulate mineralization in concert with osteoblast-specific factors such as bone gamma-carboxyglutamic acid-containing protein (BGLAP) and runt-related transcription factor 2 (RUNX2). Pyrophosphate (PPi) generated by ectonucleotide pyrophosphatase/phosphodiesterase 1 (ENPP1) is an essential suppressor of hydroxyapatite deposition and alkaline phosphatase (ALP) inactivates PPi[12]. ALP abundance is thus a central factor for local phosphate homeostasis, and during osteogenic differentiation increased ALP activity is a hallmark of the bone-like characteristics of the cells in other extra-skeletal tissue such as blood vessels. In this paper, ALP is used as an acronym for all four isozymes of ALP as all can be found in TGCTs[13]. In addition, accumulating evidence suggests that fibroblast growth factor 23 (FGF23) and its receptor Klotho, the phosphate transport proteins solute carrier family SLC34A-1, -2, and -3, and vitamin D metabolizing enzymes are essential for maintaining stable mineral homeostasis and that imbalance in their activity may lead to extra-skeletal calcifications[14–18]. Interestingly, loss-of-function variants in the *GALNT3* gene and hence a lack of degradation-protective glycosylation of FGF23 leads to systemic hyperphosphatemia and severe testicular microcalcifications[19–21]. Intratesticular phosphate levels seem to be essential in the formation of testicular microlithiasis as loss-of-function variants in the main testicular phosphate transporter *SLC34A2* also lead to severe testicular microcalcifications without affecting systemic phosphate levels[22]. Testicular microlithiasis is also found in patients with loss-of-function variants in the gene encoding ATP binding cassette subfamily C member 6 (*ABCC6*), which results in abnormal PPi metabolism and thus less inhibition of mineralization[23]. These studies indicate that particularly local and potentially systemic changes in phosphate homeostasis induce testicular microcalcifications. Therefore, we hypothesized that the etiology of testicular microcalcifications involves disturbances in intratesticular mineral homeostasis.

TGCTs originate from a common progenitor germ cell neoplasia *in situ* (GCNIS), which is characterized by the expression of pluripotency factors such as octamer-binding transcription factor 4 (OCT4), NANOG, and high alkaline phosphatase activity[13,24–27]. GCNIS cells undergo malignant transformation and form either a seminoma that retains germ cell characteristics or a non-seminoma that may contain embryonal carcinoma (EC) resembling human embryonic stem cells (hESCs), teratoma, yolk sac tumor, choriocarcinoma, or a combination of these[28]. During the malignant transformation of GCNIS into invasive TGCTs duplication of chromosome 12p (often as isochromosome 12p) is the most consistent chromosomal aberration, and may be involved in the dedifferentiation from GCNIS to EC[28]. In healthy individuals, FGF23

83 is produced exclusively in osteocytes, and the location of the gene on chromosome 12p may be important for its presence
84 and role in TGCTs. Full-length FGF23 increases phosphate excretion by decreasing the luminal expression of SLC34A1 in
85 the kidney and by lowering the concentration of active vitamin D via increased expression of the inactivating enzyme
86 CYP24A1 and reduced expression of the activating enzyme CYP27B1[29]. We have previously shown that the local
87 metabolism of vitamin D disappeared during the malignant transformation of GCNIS to EC and that FGF23 was expressed
88 in an EC-derived cell line[30]. O-glycosylation by GALNT3 protects FGF23 from rapid degradation, and full-length FGF23
89 activates a receptor complex consisting of Klotho heterodimerization with FGF receptor 1 (FGFR1). However, the cleaved
90 C-terminal fragment (cFGF23) can bind and serve as a competitive antagonist for intact FGF23 (iFGF23), and iFGF23 is also
91 capable of inducing Klotho-independent effects[31]. Loss-of-function variants in the genes *FGF23*, *GALNT3*, or *Klotho* lead to
92 tumoral calcinosis partly through osteogenic-like differentiation of mesenchymal-derived cells due to altered mineral
93 homeostasis and vitamin D metabolism[32]. Here, we investigated whether ectopic FGF23 production and abundant ALP
94 activity in TGCTs alter testicular mineral homeostasis, which alone or in combination with impaired Sertoli cell function
95 may facilitate osteogenic-like differentiation and thus be responsible for the frequent deposition of hydroxyapatite in
96 TGCTs and dysgenetic testes. To address this question, we investigated the expression of mineral regulators and bone
97 factors in human tissues containing TGCT-associated calcifications, *Fgf23* knockout (*Fgf23*$^{-/-}$) mice, hypogonadal (no
98 gonadotropins) mice, androgen-insensitive mice with microcalcifications, mice with microcalcifications due to Sertoli cell
99 ablation, mice xenografted with a TGCT-derived cell line, mice treated with a high phosphate diet, mineral deposition in a
100 mouse spermatogonial cell line (GC1), and an *ex vivo* mouse testis culture model.

101 ## Results

102 **Testicular microcalcifications are associated with the presence of renal phosphate transporters and bone markers in**
103 **human testis**

104 Ultrasonic testicular microlithiasis is often observed adjacent to TGCTs but can also be found in testes without TGCTs or
105 GCNIS (Fig. 1A). Ultrasonic testicular microlithiasis is not always associated with histological microcalcifications but
106 intratesticular mineral depositions can be confirmed by von Kossa or alizarin red staining (Fig. 1A), and Raman
107 spectroscopy has previously demonstrated that testicular microcalcifications consist of hydroxyapatite[5]. In GCNIS-
108 containing tubules adjacent to microcalcifications we found that the renal phosphate transporter SLC34A1 and FGF23
109 were ectopically expressed. In contrast, Klotho was expressed in the cytoplasm of the germ cells in normal tubules, with
110 or without adjacent microcalcifications, but not in GCNIS. FGFR1 expression was found in both GCNIS and normal tubules
111 (Fig. 1B). The expression of the bone marker BGLAP was present in tissue with GCNIS and adjacent to the
112 microcalcifications but not the normal tubules with full spermatogenesis (Fig. 1B and Suppl. Table 1). The
113 microcalcifications vary in size from small calcifications focally in the center of seminiferous tubules to occupying most of
114 the intraluminal area (Fig. 1C). In very rare severe cases there was intratesticular bone formation (Fig. 1D). We investigated
115 the presence of several bone factors in the cells adjacent to the microcalcifications. The early osteoblast marker RUNX2
116 was not expressed in testes with normal spermatogenesis. However, occasionally, when microcalcifications or bone
117 formation were detected, a small fraction of the germ cells in the seminiferous tubules (ST) had cytoplasmic staining of
118 RUNX2 supporting a bone-like phenotype of some germ cells (Fig. 1D, Suppl. Fig. 1, and Suppl. Table 1). The shift in
119 expression of the phosphate transporters from SLC34A2 to SLC34A1 and the presence of bone factors in testis with
120 microcalcifications were also evident at the transcriptional level. *SLC34A1* was expressed at a very low level in normal
121 testis but was highly expressed in 25% of the specimens containing GCNIS. In contrast, the phosphate transporter *SLC34A2*
122 was abundantly expressed in the germ cells from normal testis but the expression was lower in specimens containing
123 GCNIS (Fig. 1E).

124 **FGF23 is produced by human testicular germ cell tumors and embryonic stem cells**

125 FGF23, a potent regulator of phosphate homeostasis, is expressed in the EC-derived cell line NTera2[30], and the *FGF23* gene
126 is located on chromosome 12p which is duplicated in TGCTs and could be associated with the formation of testicular
127 microcalcifications. Thus, expression of *FGF23* was investigated in human testicular specimens containing 'normal testis'
128 (adjacent tissue to TGCT/GCNIS without presence of malignant cells), Sertoli-cell-only pattern, GCNIS, seminoma, and EC
129 with or without teratoma components. The transcriptional level of *FGF23* was highest in EC components, significantly
130 higher compared with normal testis, and was positively associated with the expression of the pluripotency factors *NANOG*
131 and *OCT4* (R=0.66, P=0.049, and R=0.61, P=0.068, respectively). Two EC specimens with polyembryoma components (the
132 most dedifferentiated structure resembling early embryonic formation) had several fold higher levels of *FGF23* (Fig. 2A-
133 B). A higher expression of *FGF23* in GCNIS compared with normal testis was also confirmed in microdissected GCNIS cells,

134 while fetal gonocytes and human embryonic stem cells (hESCs) also expressed *FGF23* (Fig. 2C). The high expression of
135 *FGF23* in hESC and EC was validated by a ~30-fold higher expression in different strains of hESC cells and the EC-derived
136 cell line NTera2 compared with normal testis (Fig. 2D). In contrast, normal testicular tissue had a high expression of the
137 receptor Klotho (*KL*), whereas the expression was low in GCNIS cells and hESC (Fig. 2C). IHC confirmed the marked
138 expression of FGF23 solely in OCT4-positive GCNIS cells that also expressed FGFR1, while Klotho was exclusively expressed
139 in normal germ cells and not found in any of the OCT4-positive cancer cells including seminoma and EC (Fig. 2E and Suppl.
140 Table 1). FGF23 was also expressed in the EC cells characterized by concomitant OCT4 expression but was virtually absent
141 in seminoma cells despite their marked OCT4 expression suggesting that the chromosome 12p duplication (occurring in
142 both seminoma and EC) alone is not sufficient to maintain FGF23 production. Western blot confirmed the presence of
143 FGF23 with two bands corresponding to the sizes of cFGF23 and iFGF23 in GCNIS and EC. cFGF23 was also expressed in
144 NTera2 cells, and neither cFGF23 nor iFGF23 were detected in normal testis or the seminoma-derived cell line TCam2 (Fig.
145 2F). cFGF23 and iFGF23 were expressed in an anaplastic seminoma sample, which is considered a rare intermediate
146 between seminoma and EC due to the high proliferative index and morphological resemblance with EC (Fig. 2F and Suppl.
147 table 1). Production and release of FGF23 in GCNIS and EC cells were examined by measuring the total FGF23 (iFGF23 +
148 cFGF23) and cFGF23 concentrations in seminal fluid from healthy men and testicular tumor patients. Healthy men had
149 undetectable iFGF23 levels in the seminal fluid, and a few (8/19) men had detectable cFGF23. A few men with GCNIS (2/7)
150 or EC (2/10) had detectable levels of iFGF23 in the seminal fluid while total FGF23 were detected in the majority (9/10) of
151 men with EC and their total FGF23 concentration in seminal fluid was significantly higher compared with healthy men (Fig.
152 2G).

153 **Testicular phosphate homeostasis in NTera2 xenograft mice is altered by FGF23-independent actions**

154 In NTera2 xenograft tumors, FGF23 was expressed in only 5-10% of tumor cells, which indicates that the phenotype of the
155 NTera2 cells changes *in vivo*. This may be caused in part by somatic differentiation of the FGF23-negative fraction
156 comprising 90-95% of the tumors, as also illustrated by the similar expression pattern of OCT4 within the tumor (Fig. 3A).
157 Human iFGF23 in serum from nude mice with tumors was 4-fold higher compared with control nude mice (Fig. 3B) and
158 thus much lower than the EC tumors samples. The presence of iFGF23 in serum and the undetectable levels of iFGF23 in
159 NTera2 cells grown *in vitro* suggests that NTera2 cells xenografted into nude mice may undergo somatic differentiation in
160 response to host stimuli and facilitate GALNT3-mediated glycosylation of iFGF23 to prevent its cleavage (Fig. 2F).
161 Interestingly, NTera2 tumor-bearing mice had significantly higher *Slc34a1* and *Bglap* expression in testis compared with
162 nude mice without tumors but no change in *Slc34a2* suggesting that the effect induced by the tumor was cFGF23 or FGF23
163 independent (Fig. 3C). Expression of the phosphate transporter *Slc34a1* in the testis was positively correlated with the
164 tumor size (R^2=0.53, P=0.012) (Fig. 3D). Exogenous treatment with iFGF23 or cFGF23 in human testis specimens cultured
165 *ex vivo* for 24 h did not change the expression of phosphate transporters or *BGLAP* (Fig. 3E), indicating that FGF23 alone
166 is not responsible for the change in expression of these genes but may be caused by other factors released or induced by
167 the tumors.

168 **Mineralization in testis and epididymis of *Fgf23*$^{-/-}$ mice and in mice treated with a high phosphate diet**

169 *Fgf23*$^{-/-}$ mice had elevated serum concentrations of calcium and phosphate, smaller testes, and often spermatogenic arrest
170 at the spermatocyte stage compared with control mice (Fig. 4A and data not shown). Testicular evaluation showed no
171 deposition of hydroxyapatite, but DMP1, OPN, and BGLAP were expressed in the cytoplasm of some germ cells in up to
172 15% of the tubules in *Fgf23*$^{-/-}$ mice and more rarely in WT mice (Fig. 4B-C). To distinguish the effects of FGF23 loss from
173 high phosphate alone, WT mice received a high phosphate diet, which showed that short-term high serum phosphate did
174 not induce testicular microlithiasis or induce any testicular changes in the expression of phosphate transporters or *Bgalp*
175 (Fig. 4D). A more severe phenotype was observed in cauda epididymis with marked mineralization in 25% of the *Fgf23*$^{-/-}$
176 mice and none of the WT mice. DMP1, OPN, and BGLAP were highly expressed in the epididymis of *Fgf23*$^{-/-}$ mice (Fig. 4E-
177 F), while DMP1 and BGLAP were not detected in the epididymal lumen of WT mice. OPN was expressed in the head of
178 sperm in both WT and *Fgf23*$^{-/-}$ mice, although it was expressed exclusively in the luminal part in the calcified section of
179 epididymis of *Fgf23*$^{-/-}$ mice.

180 **Testicular microcalcifications in hypogonadal, androgen receptor knockout, and Sertoli cell-ablated mice**

181 Testicular microcalcifications are not exclusively found in mice with knockout of phosphate transport regulators but also
182 in ~30% of hypogonadal (*hpg*) mice that lack circulating gonadotropins (follicle-stimulating hormone and luteinizing
183 hormone). The proportion of mice with testicular microcalcifications increased to ~94% in mice with concomitant global
184 loss of the androgen receptor (*AR*) (*hpg*.ARKO)[33] (schematically illustrated in Fig. 5A). Sertoli cell-specific ablation of *AR* in
185 *hpg* mice (*hpg*.SCARKO) did not augment the effect on microcalcifications in the *hpg* mice, indicating a role of AR in
186 peritubular cells (the only other cell type in the testis that express AR) or AR-expressing cells outside the testis for the
187 formation of microcalcifications. Thus, suggesting that somatic cells may be important for the bone-like trans-
188 differentiation in mice. Noteworthy, a shift in the expression of phosphate transporters was observed in the testis of *hpg*,
189 *hpg*.SCARKO, and *hpg*.ARKO mice which had higher expression of *Slc34a1* and lower expression of *Slc20a1* and *Slc34a2*
190 compared with WT mice. Thus, supporting the hypothesis that local phosphate homeostasis is involved in the formation
191 of microcalcifications in accordance with the observations in human tissues with microcalcifications. There were no
192 significant differences in *Slc20a1, Slc34a2*, and *Slc34a1* expression between *hpg, hpg*.SCARKO, or *hpg*.ARKO mice despite
193 the higher proportion of mice with microcalcifications in the *hpg*.ARKO group. However*, Bglap* was detected in testis from
194 all *hpg*.ARKO and most *hpg*.SCARKO mice suggesting that *Bglap* is expressed in mice with disturbed Sertoli cell maturation
195 with the highest expression found in *hpg*.ARKO mice which had a 94% prevalence of microcalcifications (Fig. 5B). Ablation
196 of Sertoli cells at postnatal day 18 induced substantial microcalcifications in the adult mice (80 days old) as shown by
197 alizarin red and von Kossa staining (Fig. 5C). The microcalcifications persisted when assessed in mice 1-year of age (data
198 not shown). The timing of ablation seemed to be important because Sertoli cell ablation in adulthood (after puberty) did
199 not cause microcalcifications when evaluated after 90 days but was detectable one year later (data not shown). This shows
200 that immature prepubertal cells are more prone to form microcalcifications. The formation of microcalcifications depends

201 on the presence of germ cells with stem cell potential as ablation of Sertoli cells during embryonic development, which
202 causes loss of germ cells, did not result in testicular microcalcifications.

203 **Alkaline phosphatases in TGCTs and effects of calcium, phosphate, and pyrophosphate on mineralization in a**
204 **spermatogonial cell line**

205 ALP degrades the potent inhibitor of mineralization PPi and is highly expressed in the cells of mineralized tissue. Clinically,
206 ALP expression is used as a marker for GCNIS and seminoma. Alkaline phosphatase activity was markedly higher in GCNIS
207 tubules compared with normal seminiferous tubules as determined by NBT/BCIP staining (Fig. 6A). All four types of ALPs
208 were expressed in normal testis and the expression in GCNIS with microlithiasis and seminoma was not significantly higher,
209 although some tumor specimens have marked expression of all four ALP isozymes. This shows that alkaline phosphatase
210 activity is higher in GCNIS/TGCTs and typically mediated by a combination of different isozymes rather than a single type
211 of ALP (Fig. 6B). To determine if mineralization can be induced in germ cells, the mouse spermatogonial cell line GC1 was
212 treated with increasing concentrations of calcium and phosphate, and mineral deposition was subsequently visualized by
213 alizarin red. Mineralization was already observed after co-treatment with calcium and phosphate for two days, but also
214 after seven days of treatment with calcium or phosphate alone (Fig. 6C). With a low serum phosphate concentration (0.9
215 mM), 3 mM calcium was required to obtain rapid mineralization after two days, whereas even 4 mM phosphate did not
216 induce mineralization in a normal calcium concentration (1.8 mM) after two or four days. However, an increment in
217 calcium to 2.0 mM enabled five of the six phosphate doses to induce rapid mineralization of the GC1 cells. This indicates
218 that low calcium levels are protective in the high intratesticular phosphate environment. Longer exposure (four and seven
219 days) augmented the response in a dose-dependent manner. The addition of PPi, an inhibitor of mineralization, reduced
220 mineralization, whereas co-treatment with PPi and pyrophosphatase (PPA1) that catalyzes the hydrolysis of
221 pyrophosphate (PPi) to inorganic phosphate (Pi) reintroduced mineralization (Fig. 6D). To assess the regulation of
222 phosphatase activity in germ cells, a human cell line TCam2 was used as a positive control. TCam2 is derived from a
223 seminoma and retains high expression of ectopic alkaline phosphatase, as assessed by NBT/BCIP staining, which was
224 critically dependent on an alkaline environment with marked phosphatase activity at pH 9, but not at pH 7 (Fig. 6E).
225 Staining with Fast Blue RR revealed that alkaline phosphatase activity was increased in the presence of osteogenic medium
226 compared with control medium, indicating that germ cells may increase their alkaline phosphatase activity in the presence
227 of factors that facilitate bone differentiation (Fig. 6F). However, an *ex vivo* model using wild-type mouse testicles (Fig. 7A)
228 cultured for 14 days with osteogenic medium -/+ phosphate did not change the expression of the bone markers *Bglap*,
229 *Runx2*, or *Alpl* (Fig. 7B). However, occasionally one or few tubules had expression of RUNX2, which was observed more
230 often in specimens treated with osteogenic medium than in specimens treated with vehicle (Fig. 7C). Few of the specimens
231 only had Sertoli cells in the tubules due to loss of germ cells and were therefore excluded from the analysis. Runx2 protein
232 expression was not observed in those tissue pieces.

233 We propose that the formation of testicular microcalcifications occurs because of one or more of the following events:
234 disturbed local phosphate homeostasis, decreased function of the Sertoli cells, reduction of mineralization inhibitors, or
235 aberrant germ cell function. These changes alone or in combination can drive osteogenic-like differentiation of germ cells
236 resulting in intratubular deposition of microcalcifications (Fig. 8).

Discussion

This translational study demonstrates that testicular microcalcifications, both benign and malignant, occur secondary to changes in gonadal phosphate homeostasis and are often accompanied by a subsequent osteogenic-like differentiation of germ cells or testicular somatic cells. Microcalcifications are more prevalent in testicular biopsies with GCNIS than without[34], which highlights that GCNIS or TGCTs may release factors involved in the development of microlithiasis, but the accompanied impaired Sertoli cell function appears to be of greater importance than the presence of malignant germ cells. In this manuscript, we show that impaired Sertoli cell function in both mice and humans increases the risk of testicular microlithiasis and this association seems to be more persistent than the malignant linkage.

The systemic master regulator of phosphate, FGF23, is highly expressed in GCNIS, EC, and hESC but not in classical seminoma. This suggests that the expression of FGF23 is linked with the transformation of GCNIS to the invasive EC and is not a result of duplication of chromosome 12p which is also prevalent in classical seminoma. The marked expression in EC and hESCs highlights that FGF23 is an early embryonic signal, which is further supported by the strong correlation between *FGF23* and pluripotency factors *OCT4* and *NANOG* in EC and the high *FGF23* expression in EC with polyembryoma formation. Moreover, it is in accordance with previous reports identifying *FGF23* transcripts in hESCs and during early embryonic life[35,36].

Phosphate levels in the testis are 3-fold higher than in serum[37,38]. In vascular and soft tissue calcification, FGF23-Klotho activity has been suggested to regulate ion metabolism and subsequently induce the presence of bone-like cells in the vessels[39,40]. The observed hydroxyapatite in the cauda epididymis of *Fgf23*$^{-/-}$ mice shows that loss of FGF23 signaling causes deposition of hydroxyapatite. As EC and GCNIS have no GALNT3 expression[41], FGF23 will rapidly be cleaved into cFGF23 which is in accordance with the detection of mainly cFGF23 (and not iFGF23) in seminal fluid from GCNIS and EC patients. High intratesticular cFGF23 may bind the Klotho/FGFR1 receptor and antagonize the effect of iFGF23[31] thereby inducing a phenotype resembling *Fgf23*$^{-/-}$ mice with increased expression of *Bglap*. However, in our human testis *ex vivo* model neither cFGF23 nor iFGF23 induced changes in phosphate transporters or *BGLAP* suggesting that short-term exposure (24 h) to high cFGF23 does not induce changes in phosphate transporters, bone factors, or microcalcifications. The epididymal phenotype of *Fgf23*$^{-/-}$ mice does not appear to be mediated via systemic hyperphosphatemia as a high phosphate dietary exposure for weeks did not result in testicular or epididymal microcalcifications or changes in testicular phosphate transporter expression. Instead, we have previously shown that germ cell-specific deletion of Klotho in mice leads to aberrant mineral homeostasis, particularly calcium transport through TRPV5[42], which may be important as low calcium appears to be protective for inducing microcalcifications in a high phosphate environment. Local testicular mineral levels depend mainly on the presence and activity of specific transporters and sensors of calcium and phosphate in the reproductive organs, rather than on systemic concentrations[43]. This may also explain why patients with loss-of-function variants in the predominant testicular phosphate transporter *SLC34A2* present with testicular microcalcifications[22].

269 Moreover, patients with loss-of-function variants in *GALNT3*, which lead to the early degradation of intact FGF23 to its C-
270 terminal form, present with global calcifications, severe testicular microlithiasis, and microcalcifications[19,20].

271 *Fgf23*$^{-/-}$ mice exhibit hypogonadism[44] and spermatogenic arrest, which resembles the condition of some men with
272 testicular dysgenesis syndrome that occasionally have testicular microcalcifications despite no malignancy[2,45]. Benign
273 microcalcifications may be facilitated by low levels of androgens or gonadotropins as such hormonal imbalances can
274 disrupt the Sertoli cell function. As a result, the germ cells may remain in their prepubertal stem cell state, rather than
275 maturing properly leaving them susceptible to external stimuli that could trigger abnormal differentiation. Changes in the
276 local testicular phosphate concentration (which is 3-fold higher than serum) could exert such a stimuli[37,38,46,47]. This
277 hypothesis was supported by the presence of microcalcifications in *hpg* mice with concomitant global *AR* ablation as these
278 mice have immature Sertoli cells and are unable to complete spermatogenesis[33]. Moreover, these mice had altered
279 testicular phosphate homeostasis characterized by a non-significant tendency towards lower *Slc34a2,* but significantly
280 higher *Slc34a1* expression compared with WT mice. However, both *hpg* and *hpg* mice with Sertoli cell-specific *AR* deletion
281 (*hpg.SCARKO*) had similar changes in phosphate transporters and only 30-36% frequency of microlithiasis, suggesting that
282 additional mechanisms are contributing to the formation of microlithiasis. The bone marker *Bglap* was detected
283 exclusively in all the *hpg* mice with concomitant global *AR* deletion (*hpg.ARKO*) but not in *hpg* mice with intact AR, which
284 supports that some testicular cells undergo osteogenic trans-differentiation, and this may facilitate or accompany more
285 abundant deposition of hydroxyapatite. We can not show the cell-of-origin, but we have previously shown that vitamin D
286 induces an osteogenic-like differentiation of NTera2 cells which start to express bone-specific proteins such as BGLAP[30].
287 However, the osteogenic-like differentiation in *hpg* mice occurs in non-malignant prepubertal/non-maturated testicular
288 cells although we cannot clarify the cell-of-origin.

289 Peritubular cells may be a good candidate because they are mesenchymal-derived and such fibroblast-like cells can
290 undergo osteogenic-like differentiation during vascular calcification at other sites of extra-skeletal mineralization[48].
291 However, human Sertoli cells can also form large-cell calcifying tumors[49] indicating that multiple gonadal cell types have
292 the potential to become bone-like. In mice, Sertoli cell-ablation before puberty caused extensive intratubular
293 microcalcifications[50], whereas Sertoli cell-ablation in adulthood did not result in the formation of microcalcifications when
294 assessed three months later despite a greater burden of immediate intratubular cell death. This finding is important
295 because it demonstrates that microcalcifications are not caused by massive intratubular cell death in mice but are critically
296 dependent on germ cells with stem cell potential. Thus, indicating that Sertoli cell maturation and function are essential
297 for protection against osteogenic-like differentiation of the germ cells or peritubular cells and that benign
298 microcalcifications are more likely to occur as a consequence of prepubertal Sertoli cell disturbance. The spermatogonial
299 stem cells may also be the cell type that undergoes osteogenic-like differentiation as they can spontaneously develop into
300 all three germ layers when isolated from adult mice, form teratomas in nude mice, and participate in the formation of
301 multiple organs when injected into blastocytes[51]. RUNX2 is an essential transcription factor for osteoblast development,

302 and although germ cells express a different isoform of RUNX2 (lacking exon 4-8), it is transcribed from the same promoter
303 as in bone[52,53]. RUNX2 was undetectable in healthy seminiferous tubules using an antibody targeting exon 5, but was
304 detected in GCNIS, hyalinized/calcified tissues, and the otherwise seemingly healthy seminiferous tubules adjacent to
305 bone in the testis, which could indicate that the bone-specific RUNX2 isoform may also be expressed in the testis when
306 microcalcifications occur. Also, the mature bone marker BGLAP was expressed in a fraction of cells that morphologically
307 resemble germ cells. Unfortunately, there was no cell-tracing marker in the mouse models so the required tracing
308 experiments to support that these bone-like cells originated from the germ cells could not be conducted. Instead, a
309 spermatogonial mouse cell line was exposed to calcium and phosphate at concentrations similar to those found in the
310 testis or the epididymis. After 2-7 days of exposure, the spermatogonia started to deposit minerals illustrating that they
311 developed some osteoblast-like characteristics, but they did not undergo complete osteogenic differentiation. A similar
312 experiment using an adult mouse testis culture model without exposure to gonadotropins or androgens showed that
313 treatment with an osteogenic cocktail for 14 days did not induce *Runx2*, *Bgalp*, or *Alpl* but a focal expression of the RUNX2
314 (using the antibody targeting exon 5) was found in specimens treated with both vehicle and the osteogenic cocktail,
315 indicating that RUNX2 expression was switched to the bone-specific isoform[54] during *ex vivo* culturing. Interestingly,
316 RUNX2 was more frequently found in specimens treated with the osteogenic cocktail and phosphate.

317 One of the most potent inhibitors of mineralization is PPi, which can be degraded by alkaline phosphatase or
318 pyrophosphatase[55]. PPi prevented the mineralization induced by calcium and phosphate in the GC1 cell line, which was
319 reintroduced in the presence of pyrophosphatase-degrading PPi. This highlights the role of PPi as an inhibitor of
320 spermatogonial mineralization. Alkaline phosphatases convert PPi to Pi and are expressed by primordial and malignant
321 germ cells[13,27]. Four genes encode alkaline phosphatases in humans (five in mice), and all are expressed in malignant germ
322 cells, including the tissue non-specific alkaline phosphatase (TNAP)[13]. TNAP is required for normal bone formation and
323 regulates vascular matrix mineralization by inactivation of the mineralization inhibitors PPi and OPN[56]. We show here that
324 TCam2 cells have high alkaline phosphatase activity in alkaline pH, suggesting that mineralization is promoted by
325 malignant cells. This implies that men with GCNIS and TGCTs are prone to microcalcifications due to lower PPi levels caused
326 by increased alkaline phosphatase activity. Several other inhibitors and promoters of mineralization could be involved,
327 but the marked epididymal mineralization observed in *Fgf23*$^{-/-}$ mice, despite the presence of SIBLING proteins that inhibit
328 hydroxyapatite formation and the extensive testicular microcalcifications in men with loss-of-function variants in
329 *SLC34A2*[22], suggest that a change of just one component can be enough to promote the formation of microcalcifications.
330 Bone formation in the testis is commonly observed in teratomas but can occur without malignancy. Mature bone tissue
331 formation has also been reported in the testis after trauma or bleeding without signs of GCNIS or invasive TGCTs[57]. Here,
332 we also show intratesticular bone in a specimen despite no detection of GCNIS or malignant cells. A comprehensive
333 analysis of germ cells adjacent to the bone tissue revealed focally bone-specific RUNX2 positive germ cells but none of
334 them expressed the other investigated bone markers or deposition of hydroxyapatite, which indicates that the mature

335 bone may have been formed in the interstitial compartment through a different mechanism related to the trauma rather
336 than alterations in mineral homeostasis leading to testicular microcalcifications.

337 In conclusion, we show that the formation of testicular microcalcifications occurs as a result of both malignant and benign
338 etiology, which includes one or more of the following events: aberrant function of Sertoli cells, disturbed local phosphate
339 homeostasis, change in mineralization inhibitors, and aberrant germ cell function. These changes alone or in combination
340 can drive osteogenic-like differentiation of germ cells resulting in intratubular deposition of microcalcifications consisting
341 of hydroxyapatite. Thus, this study suggests that microcalcifications alone should not be considered a marker for
342 malignancy in the testis.

343 ## Materials and Methods

344 **Human tissue samples**

345 Patients were recruited from the Department of Growth and Reproduction, Rigshospitalet, Denmark in accordance with
346 the Helsinki Declaration after approval from the local ethics committee (Permit No. H-15000931, H-17004362, KF 01 2006-
347 3472). Adult testis samples were obtained from orchiectomy specimens performed due to TGCTs. The tissue surrounding
348 the tumor contained tubules with either GCNIS cells or normal/impaired spermatogenesis. Each sample was divided into
349 fragments, which were either snap-frozen and stored at -80°C for RNA extraction or fixed overnight at 4°C in formalin or
350 paraformaldehyde and were subsequently embedded in paraffin. An experienced pathologist evaluated all samples and
351 IHC markers were used to examine the histological subtypes of the TGCT. Fetal gonads were collected after elective
352 terminations for non-medical reasons and gestational age was estimated by ultrasound at the Department of Gynecology
353 (Rigshospitalet/Hvidovre Hospital, Denmark) after approval by the local ethics committee (H-1-2012-007).

354 **Microarray**

355 For this study, the data were extracted from microarray analysis, which was performed and published in full previously[58].
356 Briefly, snap-frozen tissues were fixed in 75% ethanol and analyzed for AP-2γ (sc-12762, Santa Cruz) by IHC to identify
357 gonocytes and GCNIS and a slide was stained for alkaline phosphatase activity detectable in GCNIS and fetal germ cells.
358 Before microdissection, slides were stained with nitroblue tetrazolium (NBT)-5-bromo-4-chloro-3-indolyl phosphate
359 (BCIP). RNA was purified using Ambion RNAqueous micro kit (Applied Biosystem/Ambion). The quality of RNA was
360 evaluated using Bioanalyzer Picokit (Agilent Technologies). RNA samples were amplified in two rounds using the
361 MessageAMP™ II Kit (Applied Biosystem/Ambion). RNA was reverse transcribed using 50 ng/µL random hexamer primers.
362 Analyses were conducted on three hESCs, microdissected fetal gonocytes, microdissected GCNIS, and tissue containing
363 different percentages of GCNIS and normal testis samples. Agilent Whole Human Genome Microarray 4x44K chips, Design
364 Number 014850 (Agilent Technologies) were used for arrays. Hybridization and scanning of one-color arrays were
365 performed as described by the manufacturer and analyzed using Agilent Feature Extraction software (version 9.1.3.1).

366 **Quantitative RT-PCR (qRT-PCR)**

367 RNA was extracted from 13 tissue specimens with classical seminoma, 10 ECs where some included components of
368 teratoma, and 30 GCNIS samples (GCNIS adjacent to EC, seminoma, mixed tumor, and six GCNIS samples without an overt
369 tumor). RNA from normal testis was purified from three orchiectomy specimens with seminiferous tubules containing
370 varying degrees of full and partial spermatogenesis but with no GCNIS or tumor. Two normal testis RNA samples were
371 purchased from different companies (Applied Biosystems/Ambion and Clontech). RNA and cDNA preparation and qRT-
372 PCR were conducted as described previously[59]. qRT-PCR was performed using primers listed in Suppl. Table 3. The
373 representative bands from each primer combination were sequenced for verification (Eurofins MWG GmbH). qRT-PCR
374 analyses were performed twice in duplicates on two different plates using a Stratagene Mx300P cycler with SYBR Green
375 QPCR Master Mix (Stratagene). Changes in gene expression were determined with the comparative CT method using

376 glyceraldehyde-3-phosphate dehydrogenase (*GAPDH*) (ALP expression in human normal testis, GCNIS with microlithiasis,
377 and seminoma) or *β2-microglobulin* (*β2M*) (all other gene expression analyses) as control genes. One sample in the
378 *hpg*.ARKO group was lost during analyses, and *Slc34a1* was therefore not determined in that mouse.

379 **Western blot**

466 Frozen tissues prepared for western blot included adult normal testis, testis with GCNIS, homogeneous anaplastic
467 seminoma, EC samples, and cell lysates from NTera2 and TCam2 cells. The tissues were homogenized in RIPA lysis buffer
468 with protease inhibitor cocktail set lll (Calbiochem). After centrifugation, supernatants were collected and diluted in SDS
469 Sample buffer and heated for 5 min at 95˚C. Proteins were separated on an 8-16% gradient gel (Pierce) and transferred to
470 a PVDF membrane (Bio-Rad). The membrane was blocked in 5% milk for 1 h and incubated overnight with primary antibody
471 (diluted 1:200, #sc-16849). ß-actin was used as loading control (diluted 1:200, #sc-47778). The membranes were further
472 incubated for 1 h with an HRP-conjugated secondary antibody. Membranes were washed in TBST, and protein signals were
473 detected using 1-step NBT/BCIP (Pierce).

474 **Immunohistochemistry**

475 IHC staining was performed as described previously[60]. Briefly, antigen retrieval was conducted by microwaving for 15 min
476 in TEG or CIT buffer before incubation with 2% non-immune goat serum (Zymed Histostain kit) or 0.5% milk powder diluted
477 in TBS. Subsequently, slides were incubated with primary antibodies overnight at 4˚C (Suppl. Table 2) followed by a
478 secondary antibody, and a peroxidase-conjugated streptavidin complex (Zymed Histostain kit) was used as a tertiary layer.
479 Visualization was performed with amino ethyl carbazole. Between incubation steps, the slides were washed with TBS.
480 Counterstaining was performed with hematoxylin eosin (HE)-staining. All experiments were performed with control
481 staining without primary antibody. Staining was classified according to an arbitrary semiquantitative reference scale
482 depending on the intensity of staining and the proportion of cells stained: +++, strong staining in nearly all cells; ++,
483 moderate staining in most of the cells; +, weak staining or a low percentage of cells stained; +/-, very weak staining in
484 single cells; none, no positive cells detected.

485 **NTera2 xenografts and treatments**

486 All animal experiments were performed in compliance with the Danish Animal Experiments Inspectorate (license number
487 2011/561-1956) and conducted as previously described[30]. Mice were housed and interventions were conducted at
488 Pipeline Biotech in a pathogen-free area. NTera2 cells were grown under standard conditions in 175 cm^2 flasks and media
489 were changed every 48 hours. Matrigel (BD Biosciences) was diluted in Dulbecco's modified Eagle's medium (DMEM)
490 before being mixed 1:1 with NTera2 cells. NTera2 cells ($5x10^6$ cells) were injected subcutaneously into the flanks of male
491 nude mice 6-8 weeks-old NMRI mice ($Fox1^{nu}$, Taconic Europe). The NTera2 cells were grown on the mice for 28-56 days.
492 Tumor volumes were calculated from two tumor diameter measurements using a Vernier caliper: tumor volume = L x W
493 x ½W. If a tumor diameter of 12 mm was reached the animals were sacrificed. At the end of the study, mice were

494 euthanized according to the animal welfare euthanasia statement. Tumors, kidneys, and testes were harvested and
495 weighed, and one half was fixed in formalin and embedded in paraffin for IHC, and the other half was snap-frozen.

496 **Hypogonadal mice with androgen receptor ablation globally or specifically in the Sertoli cells and Sertoli cell-ablated**
497 **mice**

498 The *hpg* mice were bred in Glasgow and all procedures were carried out under UK Home Office License and with the
499 approval of a local ethical review committee. *hpg*.SCARKO and *hpg*.ARKO mice were generated as previously described[33,61].
500 SCARKO and ARKO mice were generated by crossing mice carrying floxed *Ar* (Ar^{fl}) with mice expressing Cre regulated by
501 the Sertoli-specific promoter of AMH (*Amh-Cre*) or the ubiquitous promoter PGK-1. *hpg*.SCARKO mice were generated by
502 crossing female $Ar^{fl/fl}$ mice heterozygous for the GnRH deletion (*hpg*/+) (C3HE/HeH-101/H) with male *hpg*/+ mice
503 expressing *Amh-Cre*. The *hpg*.ARKO was generated the same way using a *Pgk1-Cre* instead of *Amh-Cre*. The mice were
504 euthanized at 9-11 weeks of age by cervical dislocation. Sertoli cell ablated mice were generated as previously described[50].
505 Briefly, *Amh-Cre* mice were bred with diphtheria-toxin receptor (iDTR) mice, and the offspring were injected
506 subcutaneously with a single acute dose (100 ng in 50 µl) of diphtheria-toxin or with 50 µl sterile water (vehicle) at
507 postnatal day 18. The mice were euthanized on postnatal day 80.

508 ***Fgf23*$^{-/-}$ mice**

509 *Fgf23*$^{-/-}$ *mice* were generated as previously described[62]. Mice were bred in Boston and all studies were approved by the
510 Institutional Animal Care and Use Committee of Harvard. The mice were euthanized at 8 weeks of age by using carbon
511 dioxide followed by cervical dislocation.

512 **Biochemical Analyses**

513 Human iFGF23 and total FGF23 (iFGF23 + cFGF23) were measured in duplicates in batched assays using assays from
514 Immutopics (Immutopics, #60-6100, #60-6600) according to the manufacturer's instructions. The seminal fluid FGF23
515 measurements in healthy men have been published previously[42]. Total serum calcium and phosphorus levels were
516 determined using Stanbio LiquiColor Kits (Stanbio Laboratory).

517 ***In vitro* cultures**

518 hESC lines were cultured in Sheffield as described previously[63]. H7 cells with or without genomic aberrations were sorted
519 using a fluorescence-activated cell sorter (FACS) and only cells expressing the pluripotency marker SSEA3
520 (undifferentiated cells) were analyzed. GC1 cells (ATCC® CRL-2053™) were grown under standard conditions at 37˚C at
521 5% CO_2 in DMEM supplemented with penicillin (100 U/ml) and streptomycin (100 mg/ml) (Gibco), 10% FBS (Gibco,
522 #11573397), and L-glutamine (Gibco, #25030-024) (2 mM final conc.) was also added to the media. To investigate
523 calcification in the GC1 cells, the cells were grown in 24-well plates and treated with increasing concentrations of $CaCl_2$
524 and $NaH_2PO_4 \cdot Na_2HPO_4$ alone or in combination with PPi (Merck, #P8010) and/or phosphatase (Prospec, #ENZ-241). The
525 medium was changed every second day. Human and mouse testes were cultured *ex vivo* using a hanging drop culture

526 approach[64] or culture on agarose gel pieces, respectively. In human testis specimens, the effects of 50 ng/ml iFGF23 or
527 200 ng/ml cFGF23 were investigated after being added to culture media with 0.1% BSA for 24 h. In the mouse *ex vivo*
528 cultures, testis from adult 8 weeks old mice were dissected and treated with osteogenic medium in a gel-based tissue
529 model. Briefly, Agarose gels (1.5%) were cut into 8x8x8 mm^3 cube, placed in 4-well plates and soaked in culture media
530 (DMEM-F12, 1X penicillin/streptomycin, 1X insulin, transferrin and selenium supplement (ITSS), 10% fetal bovine serum
531 (FBS)) for a minimum of 24 hours before setup of tissue cultures. Mouse testis was dissected into 1.5 mm^3 pieces and
532 placed in opposite corners on each gel. The tissues were cultured for 14 days at 34 °C and 5% CO_2 in 325 µl media with
533 osteogenic medium containing 50 µg/ml Ascorbic acid (Merck, #A4544), 10 mM β-glycerol phosphate (Merck, #G9422),
534 and either -/+ 2-, 4-, or 8-mM phosphate or vehicle. The medium was changed every second day. At least three replicate
535 tissue pieces from the same mouse and treatment group were fixed in formalin followed by paraffin embedding for IHC
536 and histological analyses. Tissue was evaluated for morphology and technical quality based on HE-staining.

537 **von Kossa, alizarin red, BCIP/NBT, and fast blue RR staining**

538 For von Kossa staining of tissue sections, the paraffin sections were first deparaffinized and rinsed in ddH_2O. Sections were
539 then incubated with 1% silver nitrate solution under ultraviolet light for 20 min. Thereafter, the sections were rinsed in
540 ddH_2O and incubated with 5% sodium thiosulfate for 5 min and rinsed in ddH_2O (and sometimes counterstained with
541 Mayer's hematoxylin) and dehydrated through graded alcohol and cleared in xylene. For alizarin red staining of tissue
542 sections, deparaffinized sections were stained with 2% alizarin red solution (pH 4.1-4.3) for 5 minutes. The sections were
543 then dehydrated in acetone and acetone-xylene (1:1) and cleared in xylene. For alizarin red staining of GC1 cells, the cells
544 were washed in PBS and fixed in 10% formalin for 10 min. Thereafter, the cells were washed in ddH_2O and incubated with
545 0.5% alizarin red (pH 4.1-4.3) for 20 min protected from light with light shaking. Cells were washed 2-3 times with ddH_2O
546 and left to dry. Cryosections (10 µm) were treated with BCIP/NBT mixture for 90 sec. The BCIP/NBT mixture consisted of
547 45 µl BCIP stock solution and 35 µl NBT stock solutions in 10 ml water. Stock solutions: 50 mg/ml 5-bromo-4-chloro-3-
548 indolyl phosphate (BCIP, Sigma #B8503) in 100% dimethylformamide (Sigma #D4254) and 75 mg/ml nitroblue tetrazolium
549 (NBT, Sigma #N6876) in 70% v/v dimethylformamide/distilled water. The reaction was stopped in water (1 min). BCIP/NBT
550 staining of cell lines was performed the same way but in citrate buffer (pH=7) or relevation buffer (pH=9.2-9.5). For fast
551 blue RR staining, the cells were washed in PBS and then fixed with 3.7% formalin for 10 min. Then, the cells were rinsed
552 in PBS and stained for 15 min at RT lightly shaking and protected from light. The cells were stained for alkaline phosphatase
553 activity with Napthol AS-MX, 144 n,n-dimethylformamide and Fast Blue RR salt (Sigma #F0500).

554 **Statistics**

555 Data were analyzed using GraphPad Prism v. 8 (GraphPad Software). Gaussian distribution of all numerical variables was
556 evaluated by QQ plots. Unpaired Student's t-test was used between two groups of mice. One-way ANOVA followed by
557 Dunnett's multiple comparisons test was used to test for differences between gene expression in human normal testis
558 and tumors, *ex vivo* cultures of human and mouse testes, and between WT and the different *hpg* mouse models. Kruskal-

559 Wallis test with Dunn's multiple comparisons test was used to test for differences between levels of iFGF23 and total
560 FGF23 (iFGF23 + cFGF23) in seminal fluid from healthy men and tumor patients. For correlation analyses, residual plots
561 were evaluated to ensure the validity of the correlation analyses. As a result, linear regression analyses were used to
562 investigate the link between *FGF23* and the pluripotency genes *OCT4* and *NANOG* in EC, and between tumor size and
563 *Slc34a1* expression in kidney and testis of xenografted mice. Statistical significance was determined at the following levels:
564 not significant (ns) $p>0.05$, *$p<0.05$, **$p<0.01$, *** $p<0.001$, and **** $p<0.0001$.

565 **Acknowledgments**

566 We thank Giulio Spagnoli for the MAGE antibody. We gratefully acknowledge several urologists and pathologists of the
567 Greater Copenhagen area hospitals for their help with collecting the tissue samples. We thank Betina F. Nielsen, Bonnie
568 Håkansson, Ana R. Nielsen, and Brian V. Hansen for their skillful technical assistance. We appreciate the efforts of Carsten
569 L. Buus and Klaus Kristensen from Pipeline Biotech, who performed the xenografting. We also thank all the patients and
570 donors who took part in this study.

571 **Funding**

572 Danish Cancer Society, Forskningsrådet for sundhed og sygdom, Novo Nordisk Foundation, Aase og Ejnar Danielsens fond,
573 Hørslev Fonden, Dagmar Wilhelms fond, and Ib Henriksens fond.

574 ## References

575 1. Tan, I. B. *et al.* Testicular microlithiasis predicts concurrent testicular germ cell tumors and intratubular germ cell
576 neoplasia of unclassified type in adults. *Cancer* **116**, 4520–4532 (2010).

577 2. Pedersen, M. R., Rafaelsen, S. R., Møller, H., Vedsted, P. & Osther, P. J. Testicular microlithiasis and testicular
578 cancer: review of the literature. *Int. Urol. Nephrol.* **48**, 1079–1086 (2016).

579 3. Leblanc, L. *et al.* Testicular microlithiasis and testicular tumor: a review of the literature. *Basic Clin. Androl.* **28**, 8
580 (2018).

581 4. Barbonetti, A. *et al.* Testicular Cancer in Infertile Men With and Without Testicular Microlithiasis: A Systematic
582 Review and Meta-Analysis of Case-Control Studies. *Front. Endocrinol. (Lausanne).* **10**, 1–8 (2019).

583 5. De Jong, B. W. D. *et al.* Raman spectroscopic analysis identifies testicular microlithiasis as intratubular
584 hydroxyapatite. *J. Urol.* **171**, 92–96 (2004).

585 6. Smith, G. D., Steele, I., Barnes, R. B. & Levine, L. A. Identification of seminiferous tubule aberrations and a low
586 incidence of testicular microliths associated with the development of azoospermia. *Fertil. Steril.* **72**, 467–471
587 (1999).

588 7. Kirsch, T. Determinants of Pathologic Mineralization. *Curr. Opin. Rheumatol.* **18**, 174–180 (2006).

589 8. Boström, K., Watson, K. E., Stanford, W. P. & Demer, L. L. Atherosclerotic calcification: Relation to developmental
590 osteogenesis. *Am. J. Cardiol.* **75**, 88B-91B (1995).

591 9. Rowe, P. S. N. Regulation of Bone−Renal Mineral and Energy Metabolism: The PHEX, FGF23, DMP1, MEPE ASARM
592 Pathway. *Crit. Rev. Eukaryot. Gene Expr.* **22**, 61–86 (2012).

593 10. Martin, A. & Quarles, L. D. Evidence for FGF23 Involvement in a Bone-Kidney Axis Regulating Bone Mineralization
594 and Systemic Phosphate and Vitamin D Homeostasis. in *Advances in Experimental Medicine and Biology* (ed.
595 Kuro-o, M.) vol. 728 65–83 (Springer US, 2012).

596 11. Shanahan, C. M., Crouthamel, M. H., Kapustin, A. & Giachelli, C. M. Arterial Calcification in Chronic Kidney
597 Disease: Key Roles for Calcium and Phosphate. *Circ. Res.* **109**, 697–711 (2011).

598 12. Hessle, L. *et al.* Tissue-nonspecific alkaline phosphatase and plasma cell membrane glycoprotein-1 are central
599 antagonistic regulators of bone mineralization. *Proc. Natl. Acad. Sci.* **99**, 9445–9449 (2002).

600 13. Hofmann, M. C., Jeltsch, W., Brecher, J. & Walt, H. Alkaline Phosphatase Isozymes in Human Testicular Germ Cell
601 Tumors, Their Precancerous Stage, and Three Related Cell Lines. *Cancer Res.* **49**, 4696–4700 (1989).

602 14. Yuan, Q. *et al.* Increased Osteopontin Contributes to Inhibition of Bone Mineralization in FGF23-Deficient Mice. *J.*
603 *Bone Miner. Res.* **29**, 693–704 (2014).

604 15. Lieben, L. *et al.* Normocalcemia is maintained in mice under conditions of calcium malabsorption by vitamin D–
605 induced inhibition of bone mineralization. *J. Clin. Invest.* **122**, 1803–1815 (2012).

606 16. Golub, E. E. Role of matrix vesicles in biomineralization. *Biochim. Biophys. Acta - Gen. Subj.* **1790**, 1592–1598
607 (2009).

608 17. Komori, T. *et al.* Targeted Disruption of Cbfa1 Results in a Complete Lack of Bone Formation owing to
609 Maturational Arrest of Osteoblasts. *Cell* **89**, 755–764 (1997).

610 18. Ducy, P. *et al.* Increased bone formation in osteocalcin-deficient mice. *Nature* **382**, 448–452 (1996).

611 19. Garringer, H. J. *et al.* Two novel GALNT3 mutations in familial tumoral calcinosis. *Am. J. Med. Genet. Part A* **143A**,
612 2390–2396 (2007).

613 20. Campagnoli, M. F. *et al.* Familial tumoral calcinosis and testicular microlithiasis associated with a new mutation of
614 GALNT3 in a white family. *J. Clin. Pathol.* **59**, 440–442 (2006).

615 21. Kato, K. *et al.* Polypeptide GalNAc-transferase T3 and Familial Tumoral Calcinosis. *J. Biol. Chem.* **281**, 18370–
616 18377 (2006).

617 22. Corut, A. *et al.* Mutations in SLC34A2 cause pulmonary alveolar microlithiasis and are possibly associated with
618 testicular microlithiasis. *Am. J. Hum. Genet.* **79**, 650–656 (2006).

619 23. Vanakker, O. M. *et al.* Visceral and testicular calcifications as part of the phenotype in pseudoxanthoma
620 elasticum: ultrasound findings in Belgian patients and healthy carriers. *Br. J. Radiol.* **79**, 221–225 (2006).

621 24. Skakkebaek, N. E. Possible carcinoma-in-situ of the testis. *Lancet* **300**, 516–517 (1972).

622 25. Rajpert-De Meyts, E. *et al.* Developmental expression of POU5F1 (OCT-3/4) in normal and dysgenetic human
623 gonads. *Hum. Reprod.* **19**, 1338–1344 (2004).

624 26. Hart, A. H. *et al.* The pluripotency homeobox gene NANOG is expressed in human germ cell tumors. *Cancer* **104**,
625 2092–2098 (2005).

626 27. Jacobsen, G. K. & Norgaard-Pedersen, B. Placental alkaline phosphatase in testicular germ cell tumours and in
627 carcinoma-in-situ of the testis. *Acta Pathol. Microbiol. Immunol. Scand. - Sect. A Pathol.* **92**, 323–329 (1984).

628 28. Rodriguez, S. *et al.* Expression profile of genes from 12p in testicular germ cell tumors of adolescents and adults
629 associated with i(12p) and amplification at 12p11.2–p12.1. *Oncogene* **22**, 1880–1891 (2003).

630 29. Shimada, T. *et al.* FGF-23 Is a Potent Regulator of Vitamin D Metabolism and Phosphate Homeostasis. *J. Bone*
631 *Miner. Res.* **19**, 429–435 (2003).

632 30. Blomberg Jensen, M. *et al.* Vitamin D Metabolism and Effects on Pluripotency Genes and Cell Differentiation in
633 Testicular Germ Cell Tumors In Vitro and In Vivo. *Neoplasia* **14**, 952–962 (2012).

634 31. Goetz, R. *et al.* Isolated C-terminal tail of FGF23 alleviates hypophosphatemia by inhibiting FGF23-FGFR-Klotho
635 complex formation. *Proc. Natl. Acad. Sci.* **107**, 407–412 (2010).

636 32. Farrow, E. G., Imel, E. A. & White, K. E. Hyperphosphatemic familial tumoral calcinosis (FGF23, GALNT3 and
637 αKlotho). *Best Pract. Res. Clin. Rheumatol.* **25**, 735–747 (2011).

638 33. O'Shaughnessy, P. J., Monteiro, A., Verhoeven, G., De Gendt, K. & Abel, M. H. Occurrence of testicular
639 microlithiasis in androgen insensitive hypogonadal mice. *Reprod. Biol. Endocrinol.* **7**, 88 (2009).

640 34. Kang, J., Rajpert-De Meyts, E., Giwercman, A. & Skakkebæk, N. E. The association of testicular carcinoma 'in situ'
641 with intratubular microcalcifications. *J. Urol. Pathol.* **2**, 235–242 (1994).

642 35. Cormier, S., Leroy, C., Delezoide, A.-L. & Silve, C. Expression of fibroblast growth factors 18 and 23 during human
643 embryonic and fetal development. *Gene Expr. Patterns* **5**, 569–573 (2005).

644 36. Wei, C. L. *et al.* Transcriptome Profiling of Human and Murine ESCs Identifies Divergent Paths Required to
645 Maintain the Stem Cell State. *Stem Cells* **23**, 166–185 (2005).

646 37. Jenkins, A. D., Lechene, C. P. & Howards, S. S. Concentrations of Seven Elements in the Intraluminal Fluids of the
647 Rat Seminiferous Tubules, Rete Testis, and Epididymis. *Biol. Reprod.* **23**, 981–987 (1980).

648 38. Jenkins, A. D., Lechene, C. P. & Howards, S. S. The Effect of Estrogen Administration In Vivo on the Elemental
649 Composition of the Intraluminal Fluids of the Seminiferous Tubules, Rete Testis, and Epididymis of the Rat. *J.*
650 *Androl.* **4**, 272–275 (1983).

651 39. Memon, F. *et al.* Does Fgf23–klotho activity influence vascular and soft tissue calcification through regulating
652 mineral ion metabolism? *Kidney Int.* **74**, 566–570 (2008).

653 40. Leszczynska, A. & Murphy, J. M. Vascular Calcification: Is it rather a Stem/Progenitor Cells Driven Phenomenon?
654 *Front. Bioeng. Biotechnol.* **6**, 1–8 (2018).

655 41. Rajpert-De Meyts, E. *et al.* Changes in the profile of simple mucin-type O-glycans and polypeptide GalNAc-
656 transferases in human testis and testicular neoplasms are associated with germ cell maturation and tumour
657 differentiation. *Virchows Arch.* **451**, 805–814 (2007).

658 42. Bøllehuus Hansen, L. *et al.* Influence of FGF23 and Klotho on male reproduction: Systemic vs direct effects. *FASEB*
659 *J.* **34**, 12436–12449 (2020).

660 43. Boisen, I. M. *et al.* Calcium transport in male reproduction is possibly influenced by vitamin D and CaSR. *J.*
661 *Endocrinol.* **251**, 207–222 (2021).

662 44. DeLuca, S. *et al.* Amelioration of the premature ageing-like features of Fgf-23 knockout mice by genetically
663 restoring the systemic actions of FGF-23. *J. Pathol.* **216**, 345–355 (2008).

664 45. Rebourcet, D. *et al.* Sertoli Cells Maintain Leydig Cell Number and Peritubular Myoid Cell Activity in the Adult
665 Mouse Testis. *PLoS One* **9**, e105687 (2014).

666 46. Sharpe, R. M., McKinnell, C., Kivlin, C. & Fisher, J. S. Proliferation and functional maturation of Sertoli cells, and
667 their relevance to disorders of testis function in adulthood. *Reproduction* **125**, 769–784 (2003).

668 47. O'Shaughnessy, P. J., Verhoeven, G., De Gendt, K., Monteiro, A. & Abel, M. H. Direct action through the sertoli
669 cells is essential for androgen stimulation of spermatogenesis. *Endocrinology* **151**, 2343–2348 (2010).

670 48. Ronchetti, I., Boraldi, F., Annovi, G., Cianciulli, P. & Quaglino, D. Fibroblast involvement in soft connective tissue
671 calcification. *Front. Genet.* **4**, 1–16 (2013).

672 49. Gourgari, E., Saloustros, E. & Stratakis, C. A. Large-cell calcifying Sertoli cell tumors of the testes in pediatrics.
673 *Curr. Opin. Pediatr.* **24**, 518–522 (2012).

674 50. Rebourcet, D. *et al.* Sertoli cells control peritubular myoid cell fate and support adult leydig cell development in
675 the prepubertal testis. *Dev.* **141**, 2139–2149 (2014).

676 51. Guan, K. *et al.* Pluripotency of spermatogonial stem cells from adult mouse testis. *Nature* **440**, 1199–1203 (2006).

677 52. Ogawa, S. *et al.* Cbfa1, an Essential Transcription Factor for Bone Formation, Is Expressed in Testis from the Same
678 Promoter Used in Bone. *DNA Res.* **7**, 181–185 (2000).

679 53. Jeong, J. *et al.* Expression of Runx2 transcription factor in non-skeletal tissues, sperm and brain. *J. Cell. Physiol.*
680 **217**, 511–517 (2008).

681 54. Kanto, S., Grynberg, M., Kaneko, Y., Fujita, J. & Satake, M. A variant of Runx2 that differs from the bone isoform
682 in its splicing is expressed in spermatogenic cells. *PeerJ* **4**, e1862 (2016).

683 55. Orriss, I. R. Extracellular pyrophosphate: The body's "water softener". *Bone* **134**, (2020).

684 56. Lomashvili, K. A., Cobbs, S., Hennigar, R. A., Hardcastle, K. I. & O'Neill, W. C. Phosphate-Induced Vascular
685 Calcification: Role of Pyrophosphate and Osteopontin. *J. Am. Soc. Nephrol.* **15**, 1392–1401 (2004).

686 57. Yoneda, F., Kagawa, S. & Kurokawa, K. Dystrophic Calcifying Nodule with Osteoid Metaplasia of the Testis. *Br. J.*
687 *Urol.* **51**, 413 (1979).

688 58. Sonne, S. B. *et al.* Analysis of Gene Expression Profiles of Microdissected Cell Populations Indicates that Testicular
689 Carcinoma In situ Is an Arrested Gonocyte. *Cancer Res.* **69**, 5241–5250 (2009).

690 59. Blomberg Jensen, M. *et al.* Expression of the vitamin D receptor, 25-hydroxylases, 1α-hydroxylase and 24-
691 hydroxylase in the human kidney and renal clear cell cancer. *J. Steroid Biochem. Mol. Biol.* **121**, 376–382 (2010).

692 60. Blomberg Jensen, M. *et al.* Vitamin D receptor and vitamin D metabolizing enzymes are expressed in the human
693 male reproductive tract. *Hum. Reprod.* **25**, 1303–1311 (2010).

694 61. O'Shaughnessy, P. J., Monteiro, A., Verhoeven, G., De Gendt, K. & Abel, M. H. Effect of FSH on testicular
695 morphology and spermatogenesis in gonadotrophin-deficient hypogonadal mice lacking androgen receptors.
696 *Reproduction* **139**, 177–184 (2010).

697 62. Sitara, D. *et al.* Homozygous ablation of fibroblast growth factor-23 results in hyperphosphatemia and impaired
698 skeletogenesis, and reverses hypophosphatemia in Phex-deficient mice. *Matrix Biol.* **23**, 421–432 (2004).

699 63. Andrews, P. W., Goodfellow, P. N., Shevinsky, L. H., Bronson, D. L. & Knowles, B. B. Cell-surface antigens of a
700 clonal human embryonal carcinoma cell line: Morphological and antigenic differentiation in culture. *Int. J. Cancer*
701 **29**, 523–531 (1982).

702 64. Jørgensen, A. *et al.* Hanging drop cultures of human testis and testis cancer samples: a model used to investigate
703 activin treatment effects in a preserved niche. *Br. J. Cancer* **110**, 2604–14 (2014).

704

705 **Figure 1**

706 **Deposition of hydroxyapatite is linked with the induction of bone markers and changes in the expression of**
707 **phosphate transporters.** (**A**) Ultrasonic detection of testicular microlithiasis adjacent to a tumor (left) or in an otherwise
708 healthy testis (right). Arrows indicate testicular microlithiasis. Staining of calcifications by von Kossa and alizarin red in
709 human testis. (**B**) IHC staining of proteins potentially involved in the formation of testicular microcalcifications adjacent
710 to microcalcifications in human testis. OCT4: marker of GCNIS cells. Control: without primary antibody. Scale bars
711 correspond to 125 µm (left) and 25 µm (right). (**C**) Mild (left) and moderate (right) microcalcifications in human testis
712 stained with von Kossa. Scale bars correspond to 50 µm. (**D**) Severe bone formation in testis from a man with no known
713 history of local trauma or other predisposing factors of ectopic ossification. IHC staining with RUNX2. Scale bars
714 correspond to 1.25 mm (upper), 50 µm (lower left), and 100 µm (lower right). (**E**) Expression levels of the bone marker
715 (*BGLAP*) and phosphate transporters (*SLC34A1* and *SLC34A2*) in NT (normal testis), SCO (Sertoli-cell-only) pattern, and
716 GCNIS (germ cell neoplasia *in situ*). Data are presented as mean ± SEM. *p<0.05.

717 **Figure 2**

718 **Ectopic expression of FGF23 in human testicular germ cell tumors and embryonic stem cells.** (**A**) Expression levels of
719 the pluripotency factors *NANOG* and *OCT4*, and *FGF23* in normal testis (NT), Sertoli-cell-only (SCO) pattern, GCNIS,
720 seminoma (SEM), and EC +/- teratoma (T). (**B**) Correlations between gene expression of *FGF23* and *OCT4* or *NANOG* in EC
721 +/- T. (**C**) Microarray showing expression levels of *FGF23* and *KL* in microdissected fetal gonocytes and GCNIS compared
722 with testicular tissue samples with varying percentages of GCNIS, hESC, and NT. (**D**) Expression level of *FGF23* in NT,
723 hESC, and NTera2 cells (n=1-5). (**E**) IHC staining of GCNIS with adjacent NT, EC, and SEM. Scale bars correspond to 250
724 µm (upper panels) and 100 µm (lower panels). (**F**) Western blot of iFGF23 and cFGF23 in NT, GCNIS, anaplastic SEM, EC,
725 NTera2 cells, and TCam2 cells. (**G**) Levels of seminal iFGF23 or total FGF23 (iFGF23 + cFGF23) in healthy men or men with
726 GCNIS or EC. Parentheses on the x-axis indicate sample size. Data are presented as mean ± SEM. *p<0.05, **p<0.01,
727 ****p<0.0001. Correlations indicated by R^2.

728 **Figure 3**

729 **Change in expression of phosphate transporters and a bone marker in testis of FGF23-producing NTera2 cell tumors in**
730 **xenografted mice.** (**A**) OCT4 and FGF23 expression in the tumor on the flank of the nude mice. The scale bar
731 corresponds to 250 µm. (**B**) Serum levels of human iFGF23 in control or NTera2 cell inoculated nude mice (n=5-6). (**C**)
732 Expression level of the phosphate transporters *Slc34a1* and *Slc34a2* and the bone marker *Bglap* in testis of control or
733 NTera2 cell xenografted nude mice (n=5-6). (**D**) Correlations between tumor size and expression of *Slc34a1* in testis of
734 the vehicle and NTera2 cell xenografted nude mice (n=11). (**E**) Effects of iFGF23 (50 ng/ml) or cFGF23 (200 ng/ml) after
735 24 h in human *ex vivo* cultures of testis tissue without GCNIS. Data are presented as mean ± SEM. *p<0.05, **p<0.01.
736 Correlation is indicated by R^2.

737 **Figure 4**

738 **Mineralization in reproductive organs of *Fgf23* knockout mice.** (**A**) Serum levels of calcium and Pi in WT and *Fgf23*$^{-/-}$
739 mice. (**B**) Table of bone marker expression observed in premeiotic germ cells in WT and *Fgf23*$^{-/-}$ mice. (**C**) IHC staining of
740 bone markers and vitamin D processing enzymes in WT and *Fgf23*$^{-/-}$ mice. Scale bar corresponds to 100 µm. (**D**)
741 Expression level of the calcification-regulators *Abcc6* and *Enpp1*, the phosphate transporters *Slc34a2* and *Slc34a1*, and
742 the bone marker *Bglap* in testis of mice that received normal or high phosphate diet (n=8-10). (**E**) IHC staining of bone
743 markers and staining of minerals with von Kossa and alizarin red in epididymis of WT and *Fgf23*$^{-/-}$ mice. The scale bar
744 corresponds to 250 µm. (**F**) Table of bone marker expression observed in the epididymis of WT and *Fgf23*$^{-/-}$ mice. Data
745 are presented as mean ± SEM. *p<0.05, ***p<0.001, and ****p<0.0001.

746 **Figure 5**

747 **Testicular microcalcifications in hypogonadal and Sertoli cells ablated mice.** (**A**) Schematic representation of the
748 prevalence of microlithiasis in ARKO, SCARKO, *hpg*, *hpg*.SCARKO, and *hpg*.ARKO mice models. (**B**) Expression levels of
749 *Slc20a1*, *Slc34a2*, *Slc34a1*, and *Bglap* in testis of *hpg*, *hpg*.SCARKO, and *hpg*.ARKO mice models (n=2-4). Data are
750 presented as mean ± SEM. *p<0.05. (**C**) Microcalcifications in Sertoli cell-ablated mice. Mineral stainings with alizarin red
751 or von Kossa. Scale bars correspond to 500 µm (upper pictures) and 50 µm (lower pictures).

752 **Figure 6**

753 **Alkaline phosphatase activity in normal testis and GCNIS and calcium and phosphate induced mineralization *in vitro*.**
754 (**A**) Staining of alkaline phosphatase activity with BCIP/NBT in normal testis (NT) with adjacent tubules containing GCNIS.
755 Scale bars correspond to 1 mm (left picture) and 100 µm (right pictures). (**B**) Expression levels of the four alkaline
756 phosphatases in normal testis, GCNIS with microlithiasis, and seminoma. (**C**) Mineralization stained with alizarin red in
757 GC1 cells treated with increasing concentrations of calcium and Pi for 2, 4, or 7 days. (**D**) Mineralization stained with
758 alizarin red in GC1 cells with calcium and/or phosphate in the presence of the mineralization-inhibitor pyrophosphate
759 (PPi) and/or pyrophosphatase (PPA1) that catalyzes the hydrolysis of pyrophosphate (PPi) to inorganic phosphate (Pi) for
760 4 days. (**E**) Staining of alkaline phosphatase activity with BCIP/NBT in GC1 or TCam2 cells in pH=7 or pH=9.2-9.5. (**F**) Fast
761 blue RR staining of alkaline phosphatase activity in GC1 cells cultured in control or osteogenic medium for 14 days.

762 **Figure 7**

763 (**A**) Schematic representation of the mouse testis *ex vivo* model. (**B**) Expression levels of *Bgalp*, *Runx2*, and *Alpl* in *ex vivo*
764 mouse testis tissue culture specimens treated with osteogenic medium -/+ phosphate. (**C**) Table of the prevalence of
765 focal expression of RUNX2 in mouse testis *ex vivo* cultures with vehicle and osteogenic treatment for 14 days.
766 Representative RUNX2 staining in the *ex vivo* culture treated with osteogenic media and 8 mM phosphate. Scale bars
767 correspond to 50 µm (left picture) and 25 µm (right pictures).

768 **Figure 8**

769 **Overview of events that can contribute to the formation of testicular microlithiasis.** We suggest that the formation of
770 testicular microcalcifications occurs as a consequence of one or more of the following events: decreased function of the
771 Sertoli cells, disturbed local phosphate homeostasis, reduction of mineralization inhibitors, or aberrant germ cell
772 function. These changes alone or in combination can drive osteogenic-like differentiation of germ cells resulting in
773 intratubular deposition of microcalcifications consisting of hydroxyapatite.

774 **Supplementary table 1**

775 Immunohistochemical expression of selected proteins in human specimens

776

	n	FGF23	KLOTHO	FGFR1	BGLAP	RUNX2	OPN
Normal testis	7-15	÷	++ to +++	++ to +++	÷	÷	+
Germ cell carcinoma *in situ*	6-18	+++	÷ to +/-	++ to +++	+	+++	+
Hyalinized/calcified testis	5-14	÷ to +	+/- to +	++	+++	+++	+++
Classical seminoma	4-15	÷ to +	÷	++	÷	÷	÷
Anaplastic seminoma	2	++	+/-	++	N.A.	N.A.	N.A.
Embryonal carcinoma	4-13	++ to +++	÷ to +/-	++	+/- to ++	+/- to +	+/- to +
Teratoma	3-6	÷ to +	+/- to ++	++	+/- to ++	+/- to +	+/- to +
Fetal testis	3	÷ to +/-	÷	++	N.A.	N.A.	N.A.

783

784 ÷ Not expressed
785 +/- Barely detectable in few cells
786 + Expressed in few cells
787 ++ Markedly expressed in some cells or expressed in most cells
788 +++ High expression in most cells
789 N.A. Not available

790 **Supplementary table 2**

791 List of primary antibodies used for IHC staining.

Antibody	Catalog no.	Manufacturer	Dilution	Buffer
BGLAP	sc-30044	Santa Cruz biotechnology	1:50 / 1:100	CIT
CYP24A1	sc-66851	Santa Cruz biotechnology	1:500	CIT
CYP27B1	sc-67261	Santa Cruz biotechnology	1:100	CIT
DMP1	sc-73633	Santa Cruz biotechnology	1:100	TEG
FGF23	sc-16849	Santa Cruz biotechnology	1:75 / 1:200	TEG
FGFR1	sc-33928	Santa Cruz biotechnology	1:500	TEG
Klotho	sc-22220	Santa Cruz biotechnology	1:100 / 1:200	TEG
MAGE	Gift from Prof. Spagnoli	Non-commercial	1:500	TEG
NPT2a	sc-33928	Santa Cruz biotechnology	1:200	TEG
OCT4	sc-5279	Santa Cruz biotechnology	1:50 / 1:100	TEG
OPN	sc-73631	Santa Cruz biotechnology	1:100	CIT
ALP	M7191	Abcam	1:100	CIT
RUNX2	sc-10758	Santa Cruz biotechnology	1:200 / 1:400	TEG
SOX9	AB5535	Merck Millipore	1:400	TEG

792

793 **Supplementary table 3**

794 List of primers used for qRT-PCR

Gene	Forward primer	Reverse primer
	Human	
ALPI	TACACGTCCATCCTGTACGG	CTCGCTCTCATTCACGTCTGG
ALPL	ATGGGATGGGTGTCTCCACA	CCACGAAGGGGAACTTGTC
ALPP	CACCTGTGGGACTTGAGGAC	TTTGGCTCTCGACCAGTGTC
ALPP2	GGCATCATCCCAGTTGAGGAG	GCACATGCTTGTCTACACTGTAT
B2M	ATCCAATCCAAATGCGGCATC	AGTATGCCTGCCGTGTGAAC
BGLAP	CACTCCTCGCCCTATTGGC	GTGGTCAGCCAACTCGTCA
FGF23	CACCTGCAGATCCACAAGAA	TAATCACCACAAAGCCAGCA
GAPDH	TCAACGACCACTTTGTCAAGC	GGTGGTCCAGGGGTCTTACTC
NANOG	TGATTTGTGGGCCTGAAGAAAA	GAGGCATCTCAGCAGAAGACA
OCT4	GACTCCTCGGTCCCTTTCC	CAAAAACCCTGGCACAAACT
SLC34A1	CCCTCAGGTCCTACACAGGAT	GGAGCAGACGAAGAGGTAGAG
SLC34A2	CTGAGGCACCTGTAACCAAGA	GGAGCACACGAAAAAGTAGAGA
	Mouse	
Abcc6	GCATCGTTCAGGCTCGAGTG	CGAGGAGCGCCTGGAGTTAC
Alpl	CACGGCCATCCTATATGGTAA	GGGCCTGGTAGTTGTTGTGA
B2m	CGAGACATGTGATCAAGCATCA	TATTGCTCAGCTATCTAGGATAT
Bglap	CTGACCTCACAGATCCCAAGC	TGGTCTGATAGCTCGTCACAAG
Cyp24a1	ACACTGGCAGAGTACCACAAG	TCCAGGGTTTGATCTCTAGCC
Cyp27b1	GCACAGTTTACGTTGCCGAC	CGTTAGCAATCCGCAAGCA
Enpp1	AAGCGCTTACACTTCGCTAAAAG	TGATGGATTCAACGCAAGTTG
Runx2	AGAGTCAGATTACAGATCCCAGG	TGGCTCTTCTTACTGAGAGAGG
Slc20a1	TCATCATTGCATTTGTCTTGGCA	CGGATGGTTTCGCTCACTTTG
Slc34a1	GACAATGCCATCCTATCCAACC	GAGCCCATGATGATCGGAATG
Slc34a2	GACTGAACTGCTACCCTCCTA	ACCATTTGATCCCAGTGTCCT

795

796 **Supplementary figure 1**

797

798 **Deposition of hydroxyapatite and bone markers.** IHC staining of proteins potentially involved in the formation of

799 testicular microcalcifications adjacent to microcalcifications in human testis. Scale bar corresponds to 100 µm.

Fig. 1

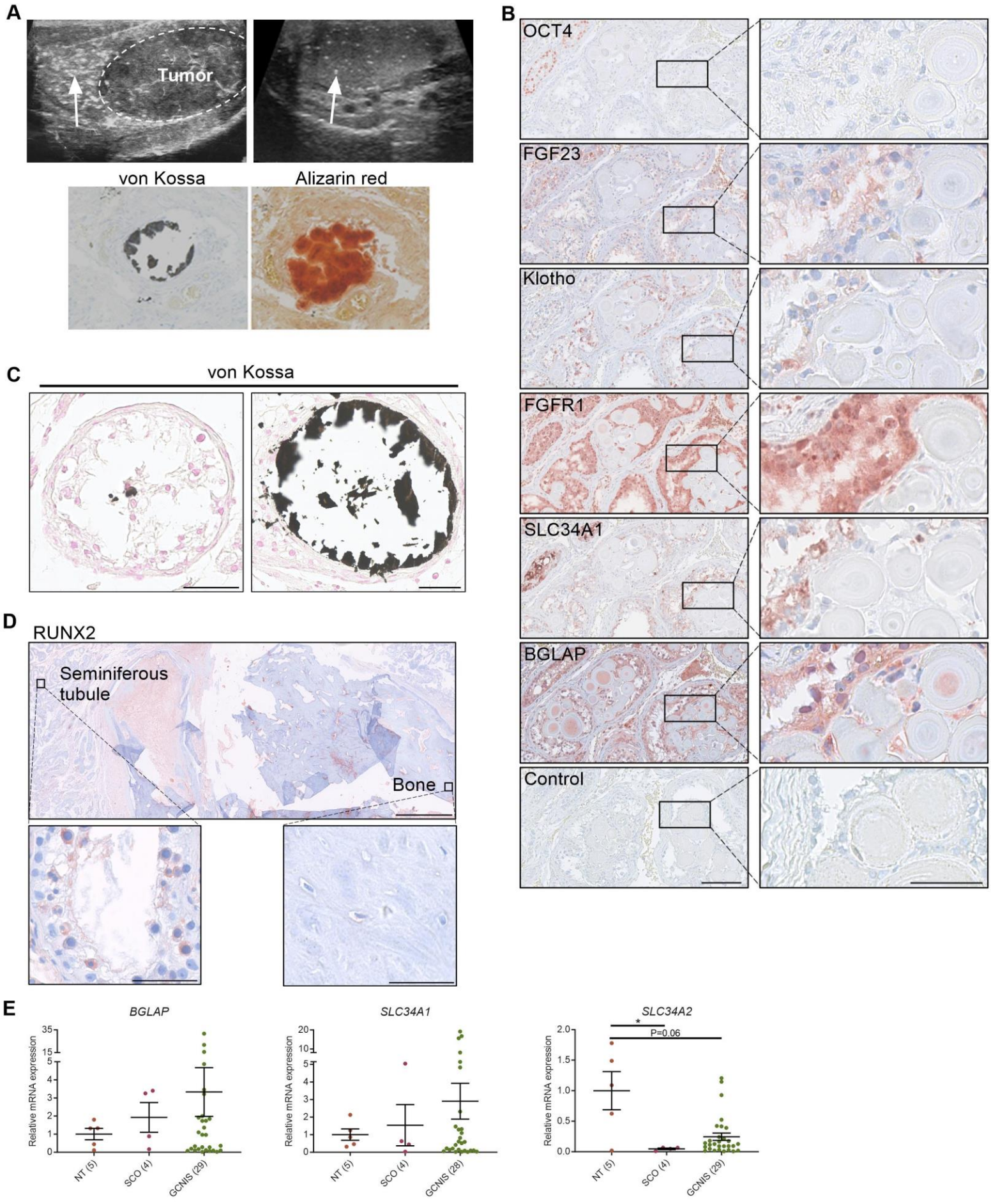
A
Tumor
von Kossa
Alizarin red
B
OCT4
FGF23
Klotho
FGFR1
SLC34A1
BGLAP
Control
C
von Kossa
D
RUNX2
Seminiferous tubule
Bone
E
BGLAP
SLC34A1
SLC34A2
Relative mRNA expression
NT (5)
SCO (4)
GCNIS (29)
GCNIS (28)
*
P=0.06

Fig. 2

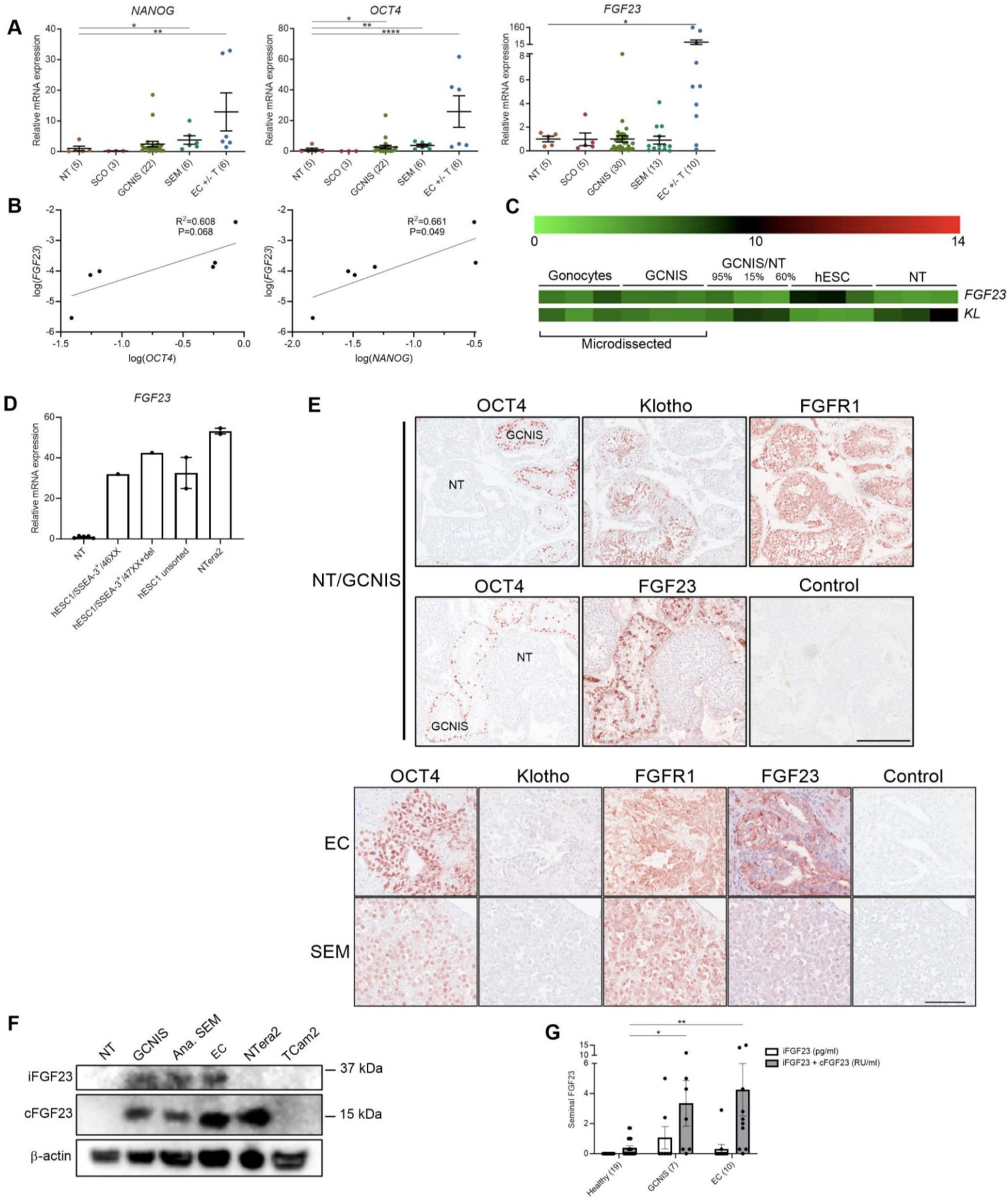
A
NANOG
OCT4
FGF23
Relative mRNA expression
NT (5)
SCO (3)
GCNIS (22)
SEM (6)
EC +/- T (6)
GCNIS (30)
SEM (13)
EC +/- T (10)
B
R²=0.608
P=0.068
R²=0.661
P=0.049
log(FGF23)
log(OCT4)
log(NANOG)
C
GCNIS/NT
Gonocytes
GCNIS
95%
15%
60%
hESC
NT
FGF23
KL
Microdissected
D
FGF23
Relative mRNA expression
NT
hESC1/SSEA-3+/46XX
hESC1/SSEA-3+/47XX+del
hESC1 unsorted
NTera2
E
OCT4
Klotho
FGFR1
GCNIS
NT
NT/GCNIS
OCT4
FGF23
Control
NT
GCNIS
OCT4
Klotho
FGFR1
FGF23
Control
EC
SEM
F
NT
GCNIS
Ana. SEM
EC
NTera2
TCam2
iFGF23
cFGF23
β-actin
37 kDa
15 kDa
G
Seminal FGF23
iFGF23 (pg/ml)
iFGF23 + cFGF23 (RU/ml)
Healthy (19)
GCNIS (7)
EC (10)

Fig. 3

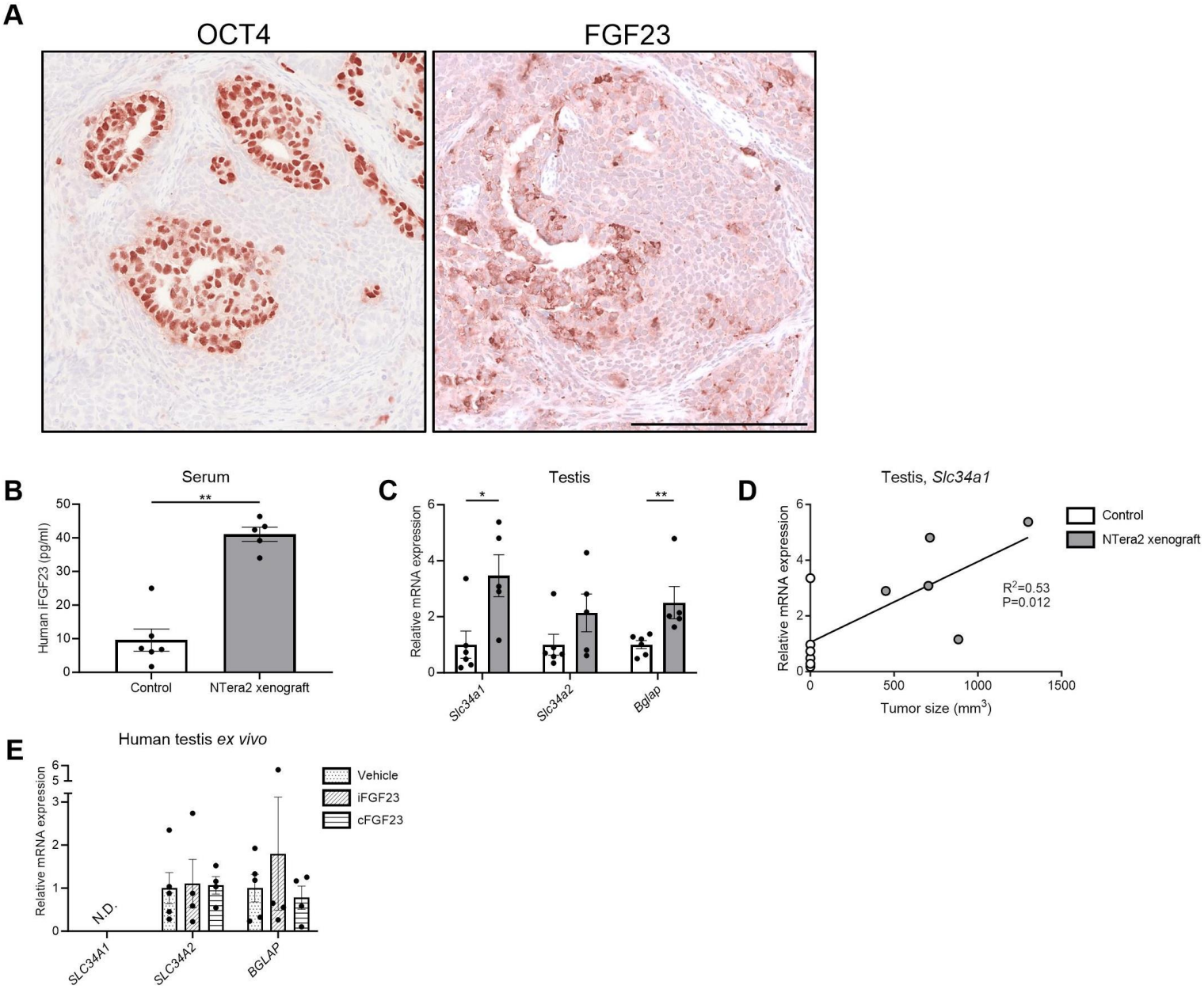
A
OCT4
FGF23
B
Serum
Human iFGF23 (pg/ml)
**
Control
NTera2 xenograft
C
Testis
Relative mRNA expression
*
**
Slc34a1
Slc34a2
Bglap
D
Testis, Slc34a1
Relative mRNA expression
Control
NTera2 xenograft
R2=0.53
P=0.012
Tumor size (mm3)
E
Human testis ex vivo
Relative mRNA expression
Vehicle
iFGF23
cFGF23
N.D.
SLC34A1
SLC34A2
BGLAP

Fig. 4

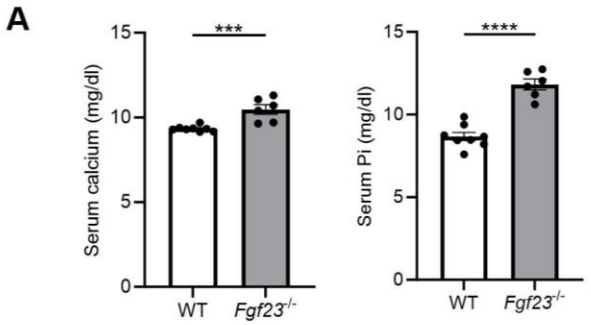

B

Premeiotic germ cells

Protein	WT	*Fgf23* $^{-/-}$
DMP1	1/4	4/4
OPN	2/5	2/2
BGLAP	1/6	4/4

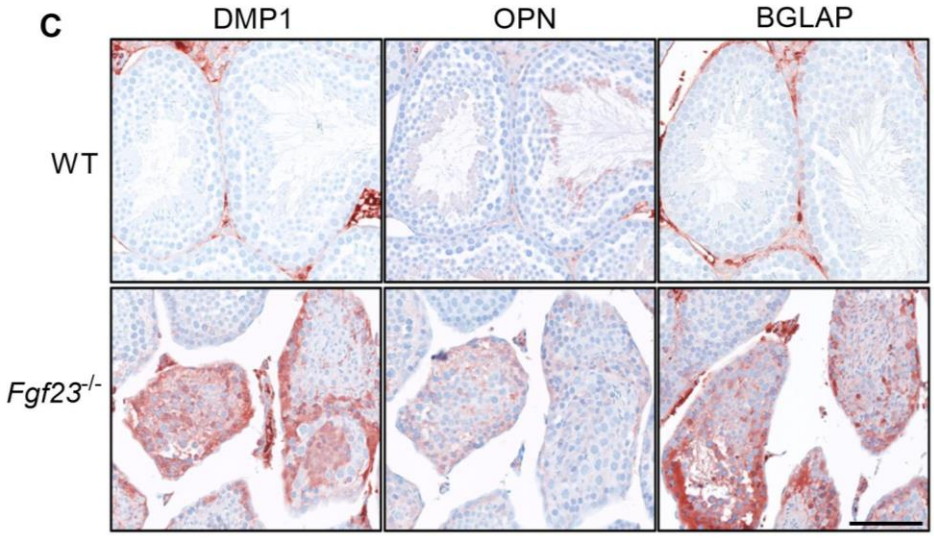

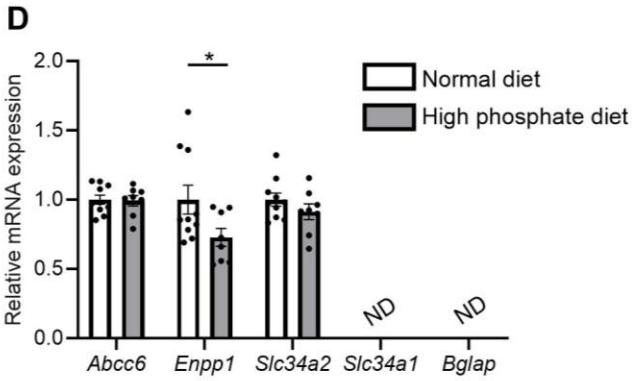

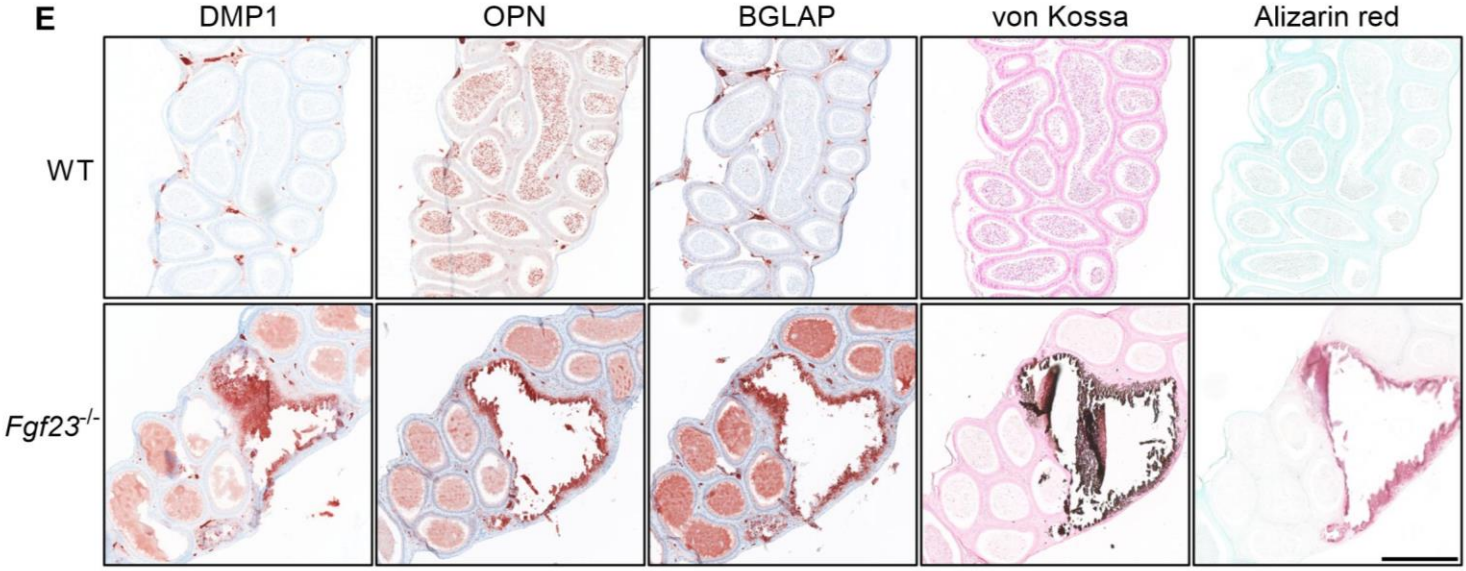

F

Epididymis

Protein	WT	*Fgf23* $^{-/-}$
DMP1	0/4	4/5
OPN	0/6	4/5
BGLAP	0/6	4/5

Fig. 5

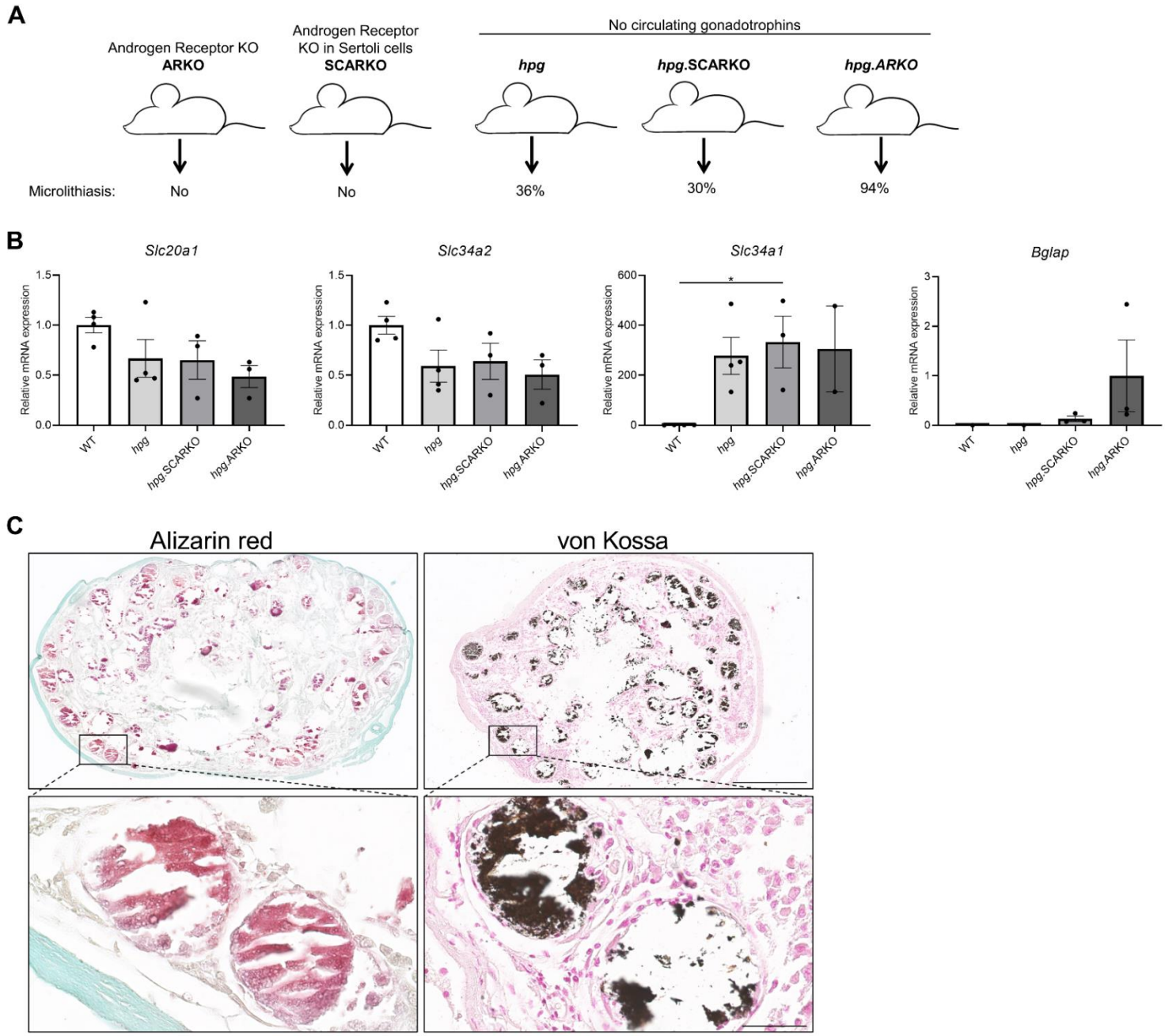
A
Androgen Receptor KO
ARKO
Androgen Receptor KO in Sertoli cells
SCARKO
No circulating gonadotrophins
hpg
hpg.SCARKO
hpg.ARKO
Microlithiasis:
No
No
36%
30%
94%
B
Slc20a1
Slc34a2
Slc34a1
Bglap
Relative mRNA expression
WT
hpg
hpg.SCARKO
hpg.ARKO
C
Alizarin red
von Kossa

Fig. 6

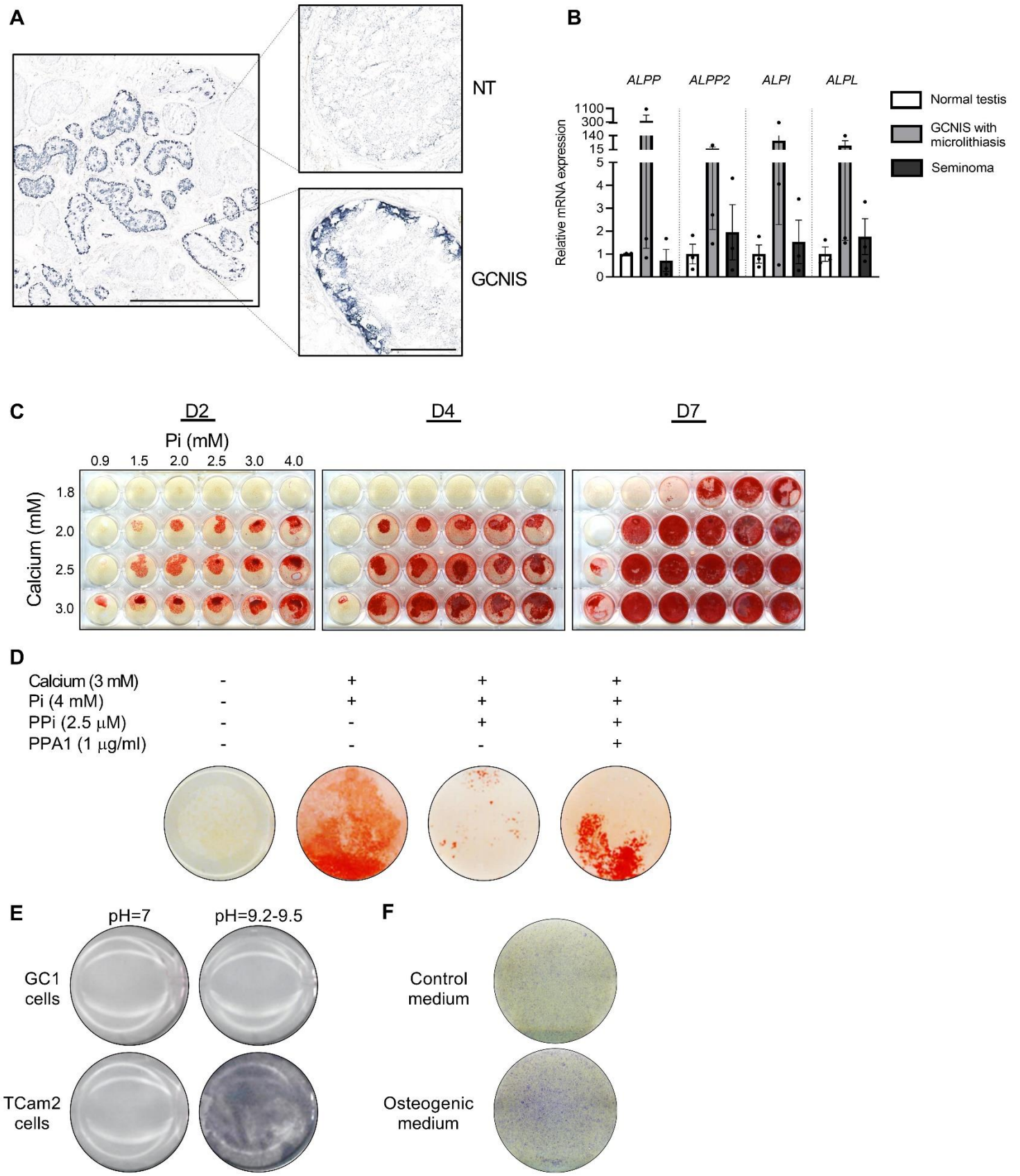
A
NT
GCNIS
B
ALPP
ALPP2
ALPI
ALPL
Relative mRNA expression
1100
300
140
15
5
4
3
2
1
0
Normal testis
GCNIS with microlithiasis
Seminoma
C
D2
D4
D7
Pi (mM)
0.9
1.5
2.0
2.5
3.0
4.0
Calcium (mM)
1.8
2.0
2.5
3.0
D
Calcium (3 mM) - + + +
Pi (4 mM) - + + +
PPi (2.5 μM) - - + +
PPA1 (1 μg/ml) - - - +
E
pH=7
pH=9.2-9.5
GC1 cells
TCam2 cells
F
Control medium
Osteogenic medium

Fig. 7

A

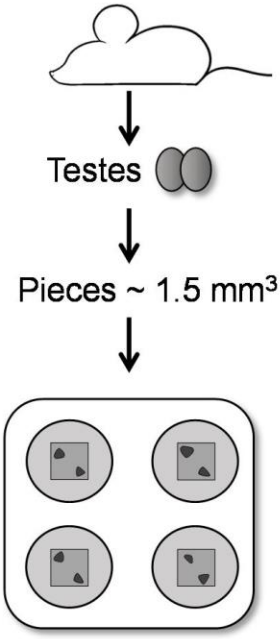

B

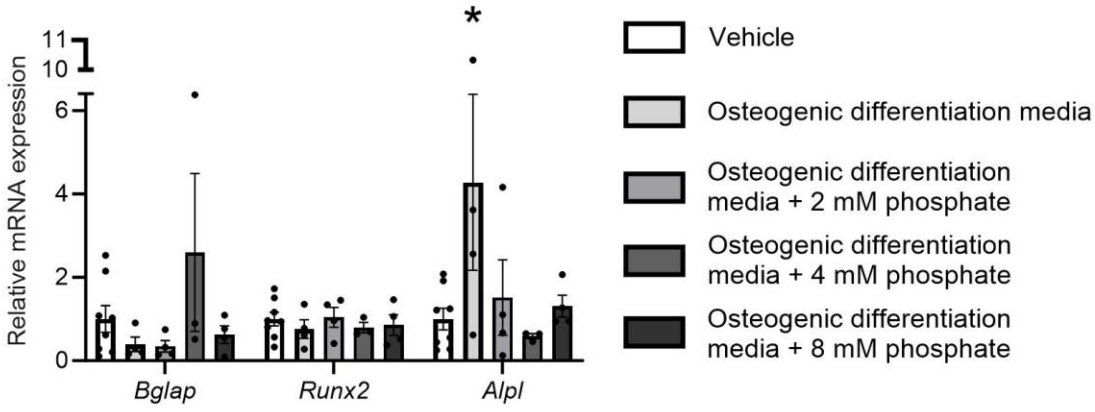

C

Treatment	RUNX2
Vehicle	2/6
Osteogenic differentiation media	2/2
Osteogenic differentiation media + 2 mM phosphate	0/4
Osteogenic differentiation media + 4 mM phosphate	4/4
Osteogenic differentiation media + 8 mM phosphate	4/4

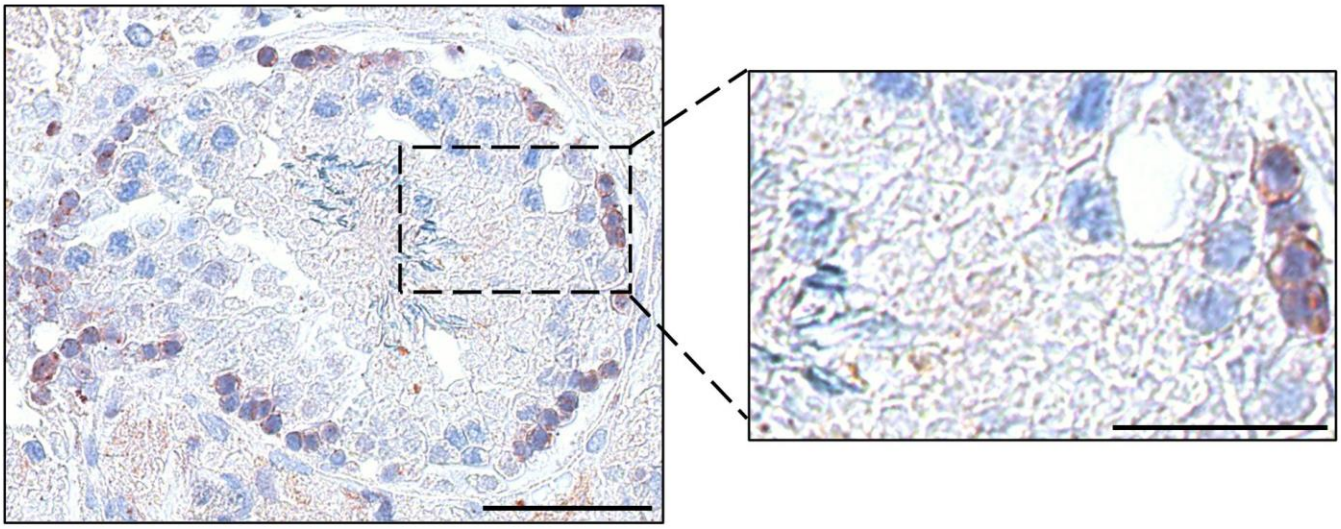

Fig. 8

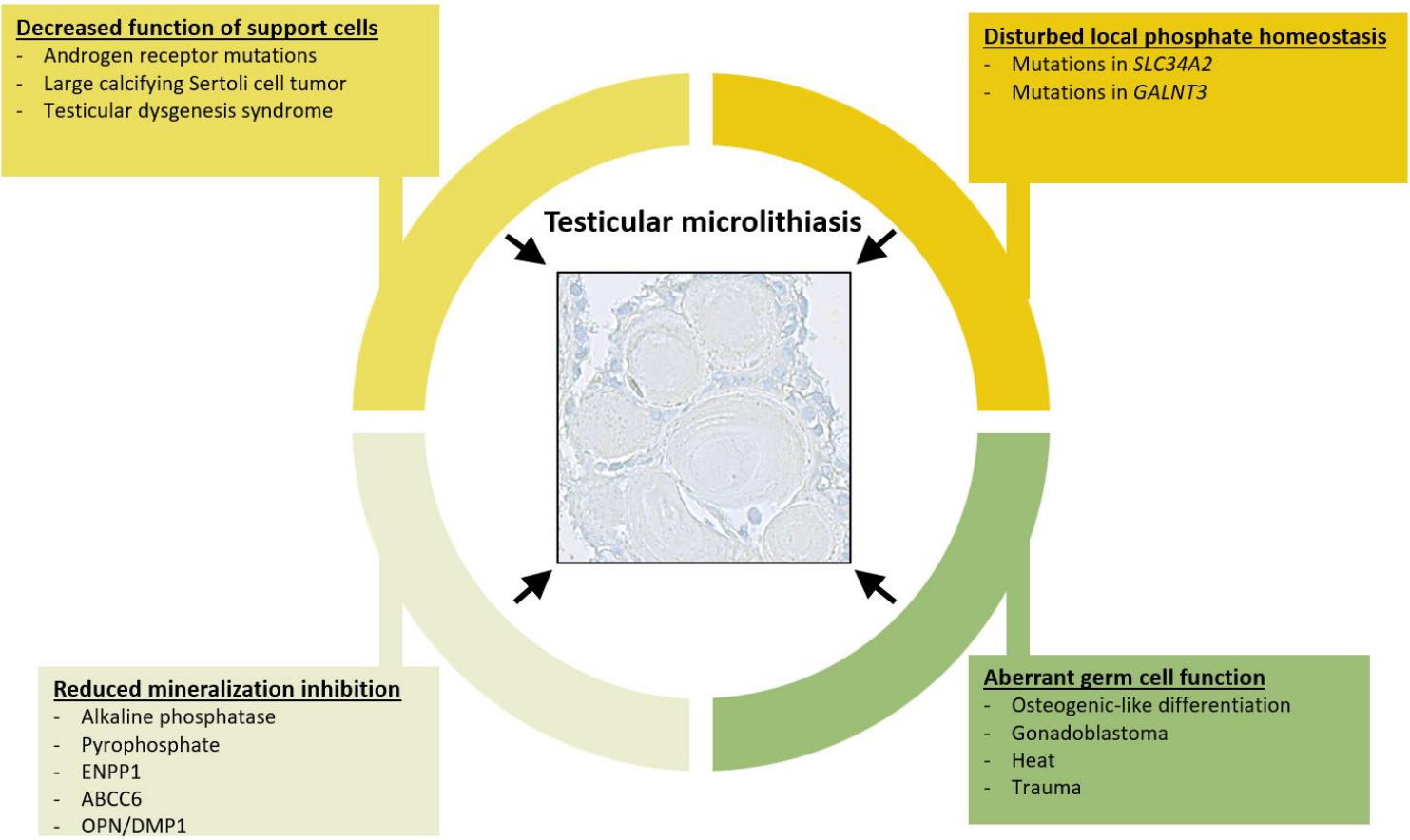
Decreased function of support cells
- Androgen receptor mutations
- Large calcifying Sertoli cell tumor
- Testicular dysgenesis syndrome
Disturbed local phosphate homeostasis
- Mutations in SLC34A2
- Mutations in GALNT3
Testicular microlithiasis
Reduced mineralization inhibition
- Alkaline phosphatase
- Pyrophosphate
- ENPP1
- ABCC6
- OPN/DMP1
Aberrant germ cell function
- Osteogenic-like differentiation
- Gonadoblastoma
- Heat
- Trauma
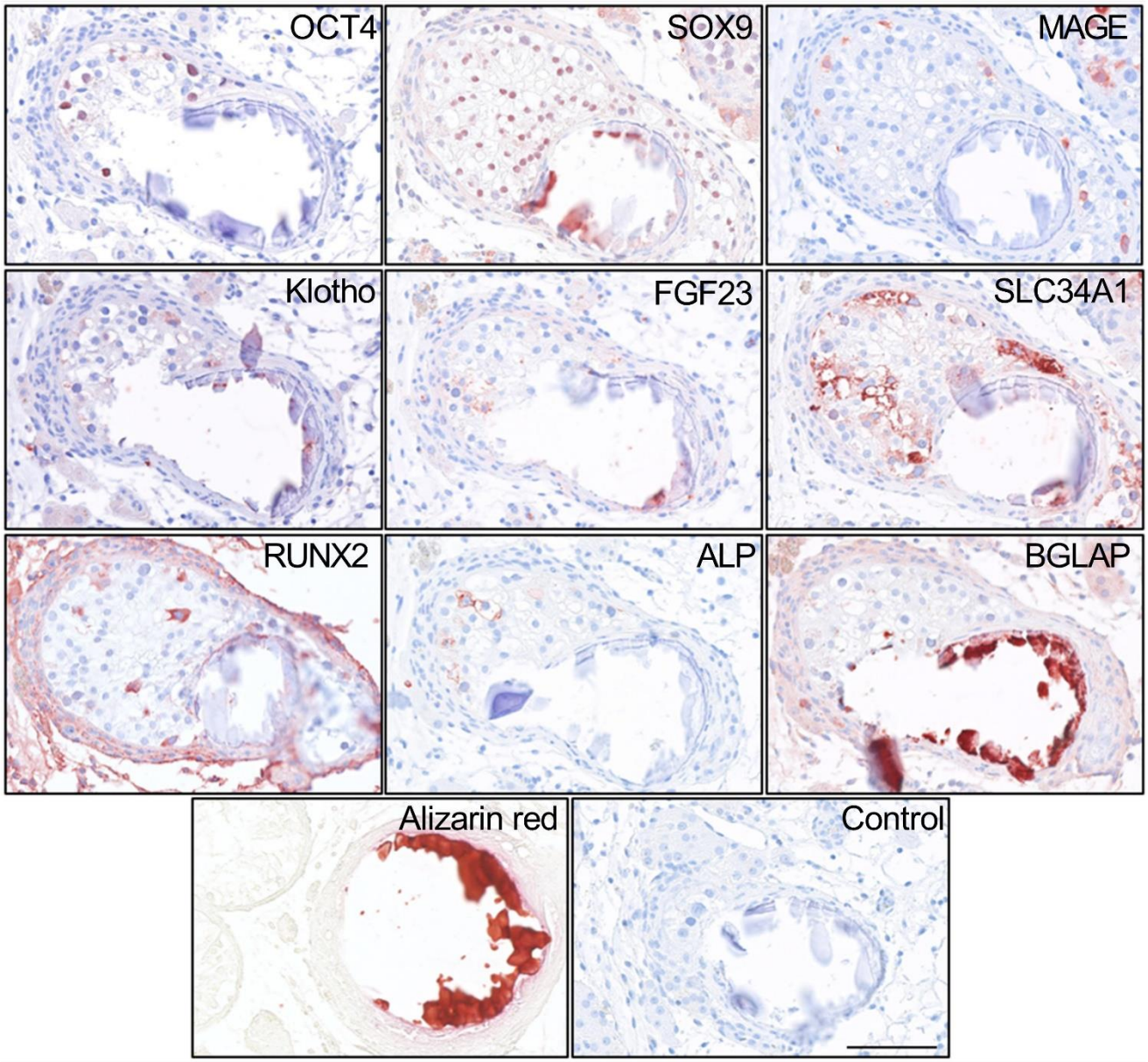
Supplementary figure 1